University of Alberta

Surface Profiling the Sanding Process of Dry Wall on Construction
by

Dony Cherian Alex

A thesis submitted to the Faculty of Graduate Studies and Research
in partial fulfillment of the requirements for the degree of

Master of Science
in
Construction Engineering and Management

DEPARTMENT OF CIVIL AND ENVIRONMENTAL ENGINEERING

Spring 2011
Edmonton, Alberta

Examining Committee

1. Dr. Zaher Hashisho (Chair and Examiner), Assistant Professor, Department of Civil and Environmental Engineering.
2. Dr. Jin-Oh Hahn (Examiner external to the department), Assistant Professor, Department of Mechanical Engineering.
3. Dr. Saeed Behzadipour (Co-supervisor and Examiner), Assistant Professor, Department of Mechanical Engineering.
4. Dr. Mohamed Al-Hussein (Co-supervisor and Examiner), Associate Professor, Department of Civil and Environmental Engineering.

Dedicated to my parents and brother.

Abstract

The growing interest in the industrialization of construction process; promotes opportunities for automation. Automation brings improvement in quality and productivity, while reducing worker's exposure to hazardous work environments. The integration of robotics in interior finishing works, such as sanding and painting of drywalls is a relatively new concept. Progressing to a stage where fully autonomous robots are used for interior finishing works requires intermediate steps; namely surface profiling. This thesis describes a theoretical concept of shadow profilometery to profile the surface of an installed drywall. A shadow was cast over the area under consideration, and the shadow profile was captured as a 2D image by a camera. Digital image processing techniques were utilized for identifying regions that deviate from a flat surface. The methodology discussed in this research, was tested on a virtual system, and the results were found to be encouraging.

Acknowledgement

"If I have seen further, it is by standing on the shoulders of giants"

It is with a feeling of profound gratitude and immense regard that I acknowledge and appreciate the valuable guidance of my supervisors. Dr. Mohamed Al-Hussein and Dr. Saeed Behzadipour, whose guidance and ideas have been of great value in the successful completion of my research.

I would like to thank Dr. Al-Hussein, for being more than just a guide, but rather a mentor, during my tenure as a Graduate Research Assistant with the Construction Engineering and Management faculty at the University of Alberta. I would also like to thank Abdullah Rabi, for aiding me with the development of my simulation models. Special thanks to Joanna Kilmowicz, for patiently correcting my writings.

To my family and close friends, whose encouragement, confidence, support, prayers and constant nagging over the years, have made such a moment possible.

There are many friends and colleagues involved; who have remained driving forces in making this research what it is today. I would like to personally thank every one of them for the humble completion of my research.

Table of Contents

List of Figures

List of Tables

Chapter 1: Introduction

1.1 Research Motivation

Research in construction automation and robotics has been gaining interest in the past two decades. The concepts behind the implementation of robotic systems in construction are similar to those currently present in manufacturing. The growth of interest in construction automation and robotics is mainly due to the solutions that its implementation provides to the problems that have been identified in the construction industry. Bock (2004) identified problems in the construction industry and classified them into the following categories:

1. Declining productivity
2. Shortage of skilled workers
3. Hazardous working conditions.

The implementation of automated and robotic systems has become more common in the automobile and other manufacturing industries, bringing about significant improvements in the productivity of these industries. The productivity in the construction industry has shown a market decline compared with other industries such as automobile and manufacturing industry. Figure 1.1 illustrates the growing gap in productivity between the automotive and construction industry, for the period of 1991 to 2000.

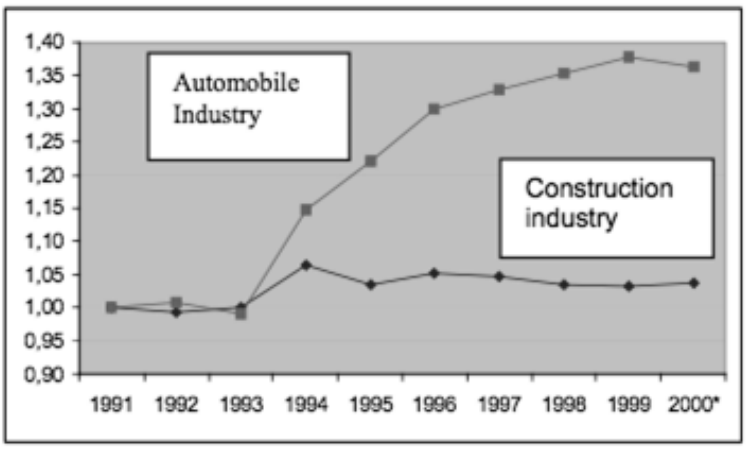

Figure 1.1: Productivity of Construction and Automobile Industry (Balaguer, 2008)

Currently, the construction of buildings has primarily been an onsite process; the nature of such an environment has many challenges. Therefore, the implementation of automated systems and robotics in this industry cannot be ignored. The main difference between other industries which employ automated solutions and the construction industry is the lack of a controllable environment on the construction site. According to research it is estimated that approximately 10 – 15% increase in overall construction productivity rate could be achieved due to automation (Skibniewski and Russell, 1989).

The uncontrollable environment in the construction industry has remained until recently, the greatest challenge in the implementation of construction automation and robotics; implementing an environment similar to the manufacturing industry could overcome such challenges. The growing interest in modular construction makes industrialization of the construction processes prospective. The pre-fabrication of building components is a well-known stage in industrialized

construction. It is expected that in the future most building components will be manufactured in fully automated factories and transported to the construction site for assembly (Kahane and Rosenfeld, 2004). Modular construction offers the advantage of a timely and reduced construction schedule, where most of the work is carried out off-site in factories under controlled conditions (Tam et al., 2007).

The conditions on a construction site often expose workers to hazardous and poor work environments. With other industries offering comparable wages, less physical work and fewer working hours, the construction industry is struggling to attract qualified workers (CII, 2003). Construction automation and robotics could reduce worker's exposure to hazardous working environments and also ensure better quality and a high standard of work. Automation and robotics constitute an integral portion of many manufacturing processes, and may be implemented with ease in the prefabrication of building components. The integration of robotics in interior finishing works, such as sanding and painting is a relatively new concept (Kahane and Rosenfeld, 2004). Progressing to a stage where fully autonomous robots are used for interior finishing works requires intermediate steps, which will gradually make this possible. Skibniewski and Hendrickson (1988), classifies basic surface operations as follows: 1) Cleaning and Shaping; 2) Coating and Spraying; and 3) Covering.

Sanding of drywalls is an interior finishing process that is categorized under cleaning and shaping. Cleaning and shaping processes are often repetitive and

hazardous tasks, which require protective equipment, continuous control, and high accuracy (Skibniewski and Hendrickson, 1988). Currently, the sanding process of drywalls is a manual process that exposes workers to ergonomic and respiratory health hazards. A report that was published by National Institute of Occupational Safety and Health indicates that drywall sanders were exposed to at least 10 times the Permissible Exposure Limits (PEL) of total dust (Miller et al., 1997). Automating this process would reduce exposure to hazardous environments, improve productivity, and improve the quality of sanding.

1.2 Research Objective

The understanding of the surface geometry becomes an important step in the development of a fully autonomous system for performing surface operations. This process of understanding the surface geometry is known as surface profiling. Surface profiling ensures proper identification of areas that require processing, and can also be used for the assessment of quality of the conducted operation.

The objectives of this research are summarized as follows:

1. Proposing a methodology for surface profiling.
2. Simulating the proposed methodology.
3. Identifying sections that deviate from normal flatness.
4. Reconstructing a 3D profile of the surface.

1.3 Thesis Organization

Chapter 2 (Literature Review) provides a review on the state-of-the-art literature that is present in the context of this research. The chapter evaluates the growing interest in construction automation and robotics. The literature corresponding to

various surface profiling techniques is also discussed in this chapter. Chapter 3 (Proposed Methodology) discusses the proposed methodology of the research. This chapter also provides a background of shadow profilometry, edge detection, and 3D reconstruction using interpolation. Chapter 4 (Implementation of Proposed Methodology) discusses the mathematical approach to the research. This chapter also discusses the case studies that were conducted in the research. Chapter 5 (Conclusion) summarizes the research and discusses its contributions, limitations, and scope for future research.

Chapter 2: Literature Review

This chapter summarizes the state-of-the-art literature related to construction automation and robotics. The literature in general comprises of reviews of the use of automation and robotics in the field of construction, the methods of surface quality inspection, and the various sensors that are used.

2.1 Robotics in the Construction Industry

Over the years, the construction industry has been one of the largest contributors to the economy and provides significant scope for innovation and further growth. However, there are a few challenges which are posed to growth of the construction industry. Bock (2004) classified current problems of the construction industry declining productivity, shortage of skilled workers, and working conditions. In a study conducted by Haas et al. (1995), it was suggested that the implementation of an automated system would enable a greater degree of flexibility in the construction industry, while reducing labor requirements, improving safety, and increasing productivity. Skibniewski and Russell (1989) estimate a 10 – 15% increase in overall productivity with the implementation of robots in the construction environment. Adapting robotic technology to construction processes is not free from challenges. Bernold (1987) addresses three aspects that concerning the future of robotics in the construction industry: 1) Needs and potential of automation and robotics at an operational and economic level; 2)Adaptability to existing technologies; and 3) Experimentation and analysis of potential processes.

The trend in research and development in the field of automation and robotics in the construction industry was studied by Son et al. (2009) and it was found that there has been a significant growth of research in applications of robotics and automated systems in the construction industry. Such conclusions were also supported by the analysis of papers that were submitted to the International Symposium on Automation and Robotics in Construction (ISARC) over the period of 1990-2008; as shown in Figure 2.1. Nearly 3000 authors from 55 countries submitted papers over this period. The distribution of papers among the countries is shown in Figure 2.2.

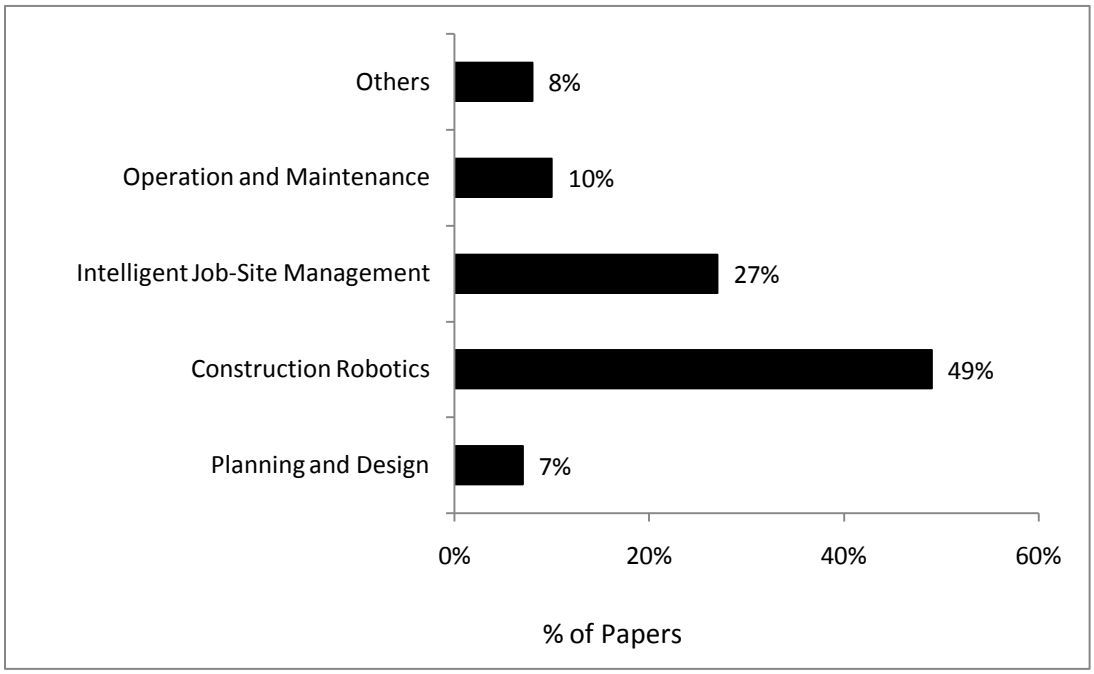

Figure 2.1: Distribution of papers by category (Son et al., 2009)

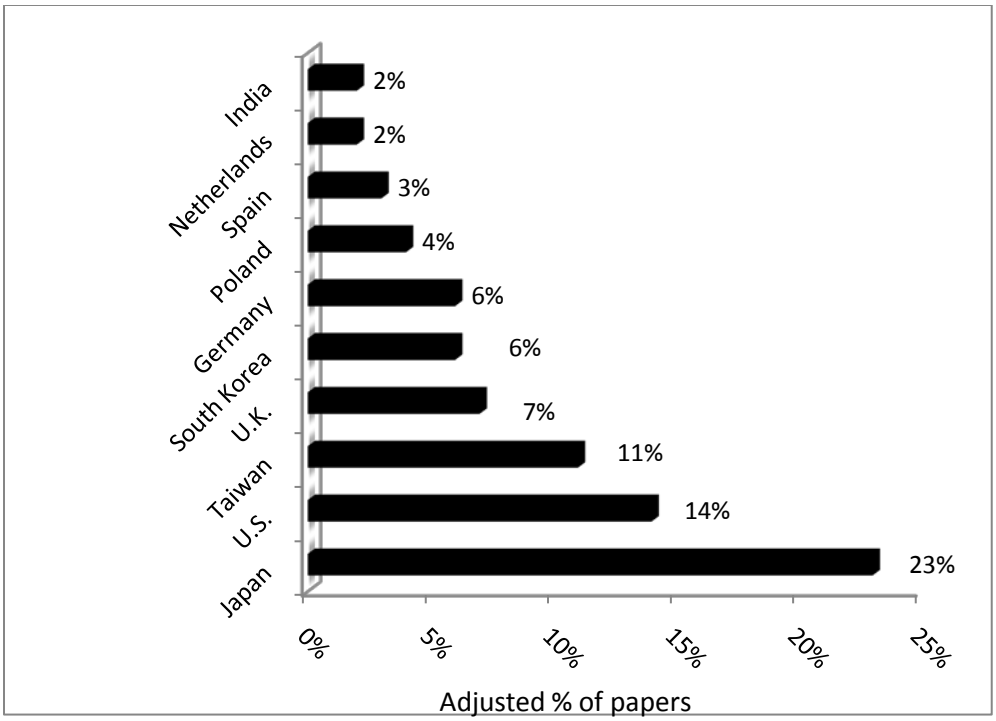

Figure 2.2: Distribution of papers by country (Son, et al., 2009).

As can be seen in Figure 2.2, research in construction innovation has been predominantly carried out in Japan; since 1980, considerable development has taken place in automated constructed technologies in Japan. More than 150 robots have been developed in the field of building construction (Arai, 2005). Bock (2004) reported that in the production line of Sekisui Chemical Sekisui Heim, in which more than 85% of the houses are prefabricated, the use of robots is substantial. Neelamkavil (2009) has also reported several automation technologies relevant to construction. A less optimistic view for the implementation of robotics in construction has been voiced by Poppy (1994), who identified obstacles in the future implementation of robotics such as: 1) High cost of automated systems; 2) Shortage of public money for research and development; and 3) Problems of acceptance.

In the research conducted by Bock (2007), various robotic implementations in the recent years were absorbed based on succesful transfer of manufacturing technology, by Toyota Homes from the automobile industry to the construction industry. Bock (2007) reported the ability to achieve affordable costs in addition to achieving human-oriented working conditions and uniform quality by the implementation of robotic solutions. Figure 2.3 and Figure 2.4 represent sample robotic processes which are currently employed in the construction industry.

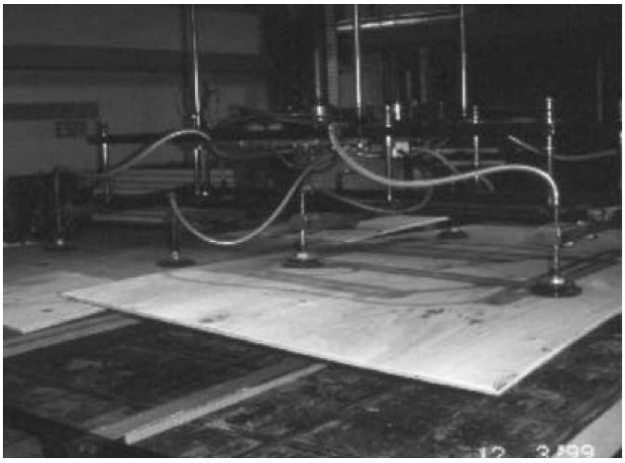

Figure 2.3: Vacuum gripper used in wood panel production.(Bock, 2007)

Figure 2.4: Overview of a factory with robotic nailing bridges (Bock, 2007)

2.2 State-of-the-art research on Automated Surface Profiling

Surface quality is of importance in drywall finishing processes. The literature that is available on automated surface profiling spans across different industries; in the construction industry, however, surface finishing tasks on installed drywalls such as painting and sanding are carried out manually; there is potential for the automation of surface profiling. Sandak and Tanaka (2005) determined that the most common technique for evaluating machined surfaces to date is human inspection; one of the most common ways of profiling is by the sense of touch, as shown in Figure 2.5.

Figure 2.5: Manual process of assessing surface smoothness.

Another common method employed in manual assessment is creating a shadow, since irregular surfaces generate shadows when exposed to light. Manual assessment is a highly subjective way of assessing quality and it is often prone to errors resulting from human fatigue and judgment (Islam et al., 2007). From the characteristics of these surface-finishing tasks, Skibniewski and Hendrickson

(1988) determined the possibility of replacing these manual tasks by robotic control strategies. Physically, surface-profiling methods can be broadly classified into two main categories: “contact based” and “non-contact based”. In principle, however, they span across a wide range of methods, including *stylus*, *optical*, *ultrasonic*, *capacitive* and *inductive* techniques (Huynh and Fan, 1992).

The most common techniques for profiling a surface is the use of a stylus, as shown in Figure 2.7. Stylus based operations exhibit a high resolution, and are generally suited for most surfaces. Sherrington and Smith (1988) listed the limitations of the stylus instruments as follows: 1) Stylus instruments only provide information pertaining to a profile section of a surface; 2) Being a contact-based approach, the pressure between the tips of the stylus and the surface, may result in damage to the surface; and 3) The operational speed of the stylus instrument is relatively slow.

Figure 2.7: Surface measurement using a stylus.

Surface profiling techniques based on other principles have also been developed. McDonald (1978) suggested the use of an ultrasonic technique for evaluating the surface of lumber. Image spectrograph methods have also been used to study the surface of wood (Hagman, 1997). Also an automatic roughness measurement

system, using a capacitive acceleration sensor, was developed for measuring the roughness of roads. The sensor would measure vertical accelerations as it moves over the road (Seppä and Heilckila, 2009).

Shadow profilometry, however, is considered to be one of the most efficient and scale independent methods for 3D characterization of a surface (Maerz et al., 1990). Huynh and Fan (1992) conducted a study of the different methods of surface profiling and provided a comparison as listed in Table 2.1.

Table 2.1: Comparative study of different surface roughness measurement techniques (Huynh and Fan, 1992).

Technique	Resolution (μm)	Speed	Cost
Stylus	1(H) 0.05(V)	Low	Medium
Interferometer	2(H) 0.0001(V)	Low	High
Focus Detection	1(H) 0.001(V)	High	Medium
Shadow graph	2	High	Low
Sectioning	1	High	Low
Scattering	0.1	Low	Low
Ultrasonic	0.5	Low	High
Capacitance	1	Low	Low
Resistance	1	Low	Low

Among the various principles discussed, the generally preferred methods for measurement are non-contact-based. There is a growing interest in the use of sensors in other operations in the construction industry; in a review of contributions to the International Symposium on Automation and Robotics in Construction (ISARC) over the period of 1990-2008, 49% of papers submitted were under the category of construction robotics, 4% of which focus on sensory systems (Son et al., 2009). A number of non-contact-based sensors have been developed and tested; however, almost no research has been conducted on evaluating the surface of drywalls. Whitehouse (1987) conducted extensive research on different surface profiling techniques. The drywall surface, which is to be profiled, is typically, a static surface. Whitehouse (1987) maps the relation between the surface measurement and manufacturing process in a factory setting as shown in Figure 2.6.

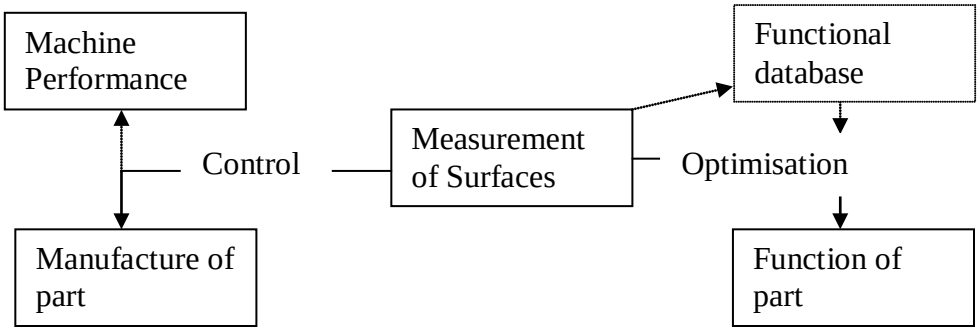

Figure 2.6: The relationship between measurements, the manufacturing process and the work piece (Whitehouse, 1987).

Knowledge of the surface is valuable in determining the parameters, such as: force, location, speed etc. that influences the performance of an automated

operation. A feedback process enables optimization, thus providing better performance in successive cycles of operation. Often, the texture of machined surfaces have a great influence on the service performance (Griffiths, 1994). The research mapped in Figure 2.6 finds a parallel in the wood industry; surface smoothness is considered as one of the most important parameters in the wood industry. The increase of emphasis on customer-oriented quality resulted in a growing interest in research relating to product smoothness. Sandak and Tanaka (2005) described the use of a shadow scanner for surface profiling in the timber industry to assess the quality of machine cutting. Altering the cutting speed provides smoother results. Shadow profiling techniques have also been employed in the rock industry (Maerz et al., 1990).

Quality control in the ceramic industry is a difficult, labor-intensive process that is usually carried out in harsh conditions. Computer vision, which incorporates the use of image processing and morphological techniques, is used to assess quality (Elbehiery, 2005). Machine vision is also utilized in the textile industry, where a combination of computer vision and neural networks is employed to identify and classify textile defects (Islam et al., 2006).

Chapter 3: Proposed Methodology

3.1 Introduction

This chapter summarizes the basic concept of shadow profiling and its implementation in determining the surface profile of an installed drywall. The proposed methodology is discussed in this chapter. This chapter also introduces concepts of edge algorithm and 3D reconstruction of surfaces using linear interpolation.

3.2 Background of Shadow Profilomtery

Shadow profilometry is the technique of tracing a surface profile, by the use of shadows. A shadow can be defined as that region which is obstructed from a light source by an object. Shadow regions have a lower intensity than the remaining regions, which are illuminated by light. It is this difference in intensity that is used for detecting edges. The cross section of a shadow is a 2D profile. When using shadow edges for surface metrology, the sharpness of the shadow becomes a major concern. The sharpness of the shadow is a function of the light source employed.

The principle behind shadow profilometry is that, when a plane of light is made to intersect with an irregular surface at an angle, the resultant intersection line follows the topography of the surface (Maerz and Hilgers, 2010). Moving laterally across the surface, multiple profiles of the surface can be obtained. A combination of these profiles can then be used to recreate a 3D profile of the

surface. If the surface under consideration is flat, then the shadow cast by a straight edge would remain a straight line. However if the surface was irregular, then the shadow would follow a corresponding curve. The principle of shadow profilometry is illustrated in Figure 3.1 and Figure 3.2, where the shadow edge follows the topography of an irregular cardboard and wooden surface respectively.

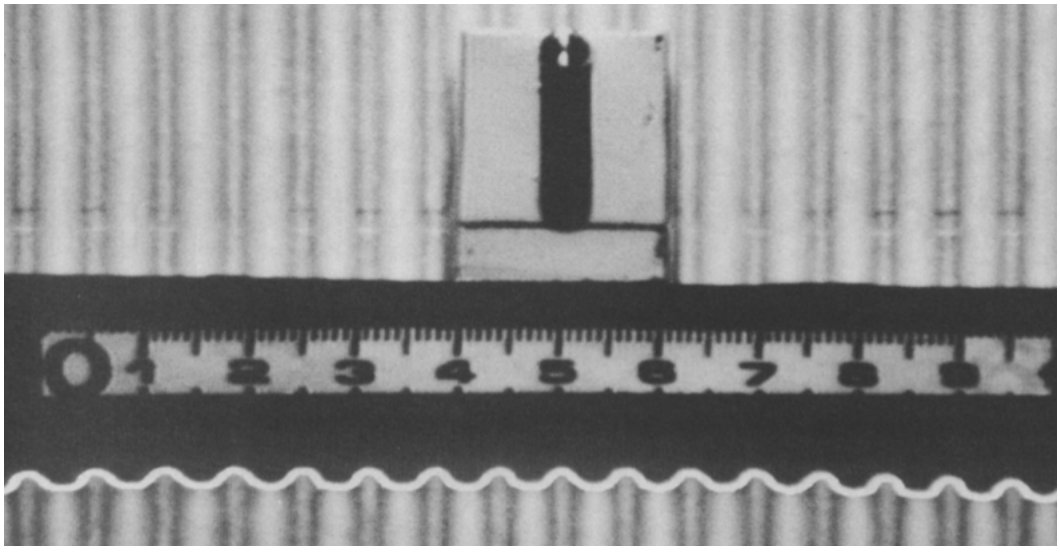

Figure 3.1: Principle of shadow profilometry highlighting the topography of irregular cardboard surface (Maerz et al. , 1990)

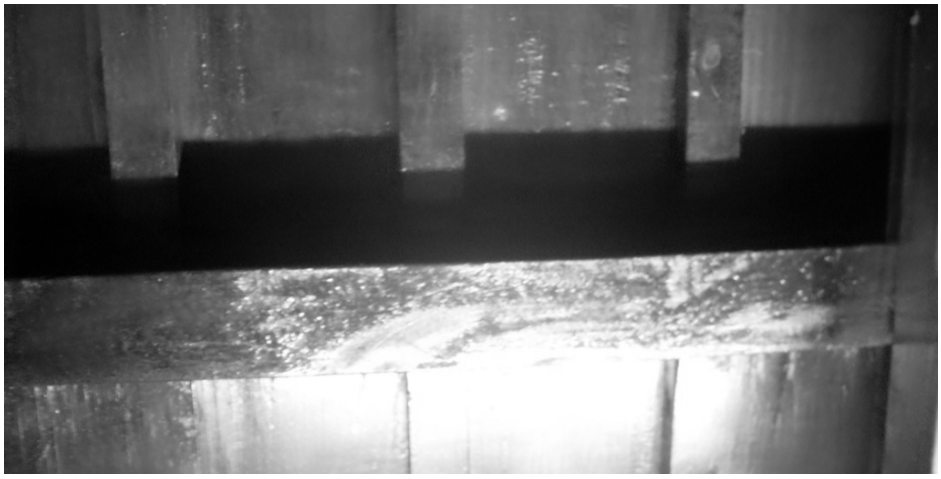

Figure 3.2: Shadow profilometry highlighting the topography of an irregular wooden surface

The use of shadow profilometry has also been described in the wood industry. Sandak and Tanaka (2005) gives a vivid description on the shadow scanner that was employed in their research. The methodology followed in this research is similar to Sandak and Tanaka's methodology. Their hardware setup comprised of a parallel light projector (1), a curtain (3) and a charge coupled device (CCD) video camera (4), which were arranged as illustrated in Figure 3.3.

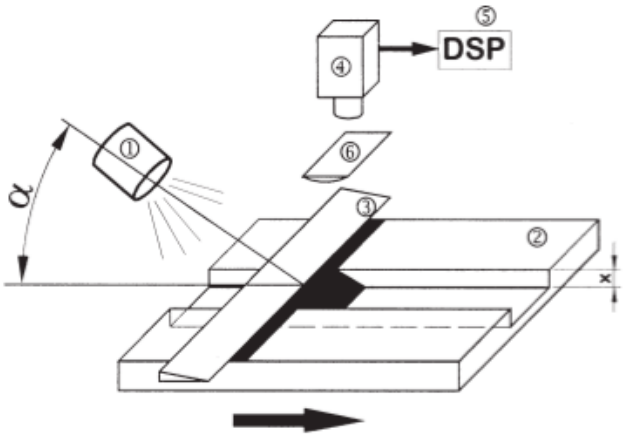

Figure 3.3 : Shadow scanner for evaluating surface smoothness in wood industry (Sandak and Tanaka, 2005).

With reference to the image above, the light is directed towards the surface at an angle 'α'. Cylindrical lenses (6 in the Figure 3.3) are utilized to improve the optical resolution. A curtain, which is above the surface, obstructs the light source and casts a shadow onto the surface. An overhead charge coupled device camera, which is placed perpendicular to the surface and aligned with the curtain, is used to capture the image of the shadow profile which is created. The edge of the shadow, which is the line that borders the dark and bright regions of the shadow, is identified using the digital signal processor (DSP) (5 in the Figure 3.3). The

image captured by the overhead camera represents one section of the surface. In the described setup, the surface is placed on a conveyor-based system. Multiple profiles of the surface are captured by the overhead camera, as the surface moves laterally ahead. The images are then individually analyzed. The results of the analysis are assimilated and used to reconstruct the 3D Profile.

Taking into perspective the conditions of a drywall and the sanding process, a few modifications were made to adapt this procedure to the current research. Since drywalls are large in size and require careful handling, the drywall is kept stationery. The sensory equipment, which comprises of the light source, curtain and the camera, is moved across the drywall surface, using either a railing or a robotic arm. Distance measurement sensors can be used to trace the location of the sensory equipment at any given time.

To avoid any contact that may damage the surface of the drywall, the curtain is placed 2 cm above its surface. Though the surface has some irregularities following the application of the third coating of the joint compound over the surface, it is safe to assume that there would be no elevation in the order of 2 cm on the surfaces.

3.3 Proposed Research Methodology

The methodology for the main process of surface profiling using shadow profilometry is illustrated in Figure 3.4. The methodology illustrated in Figure 3.4 incorporates input parameters such as the drywall surface geometry, the angle of

incidence of the light, and various parameters of the sensor. Information regarding the type of the light source used, the camera resolution, and the crispness of the shadows formed are taken into consideration in the pre-image processing phase of the computational logic. The outputs generated, will provide valuable information regarding the surface profile and its deviation from a flat surface. The main process illustrated in Figure 3.4 is comprised of two phases, namely, the test setup and the image processing algorithm.

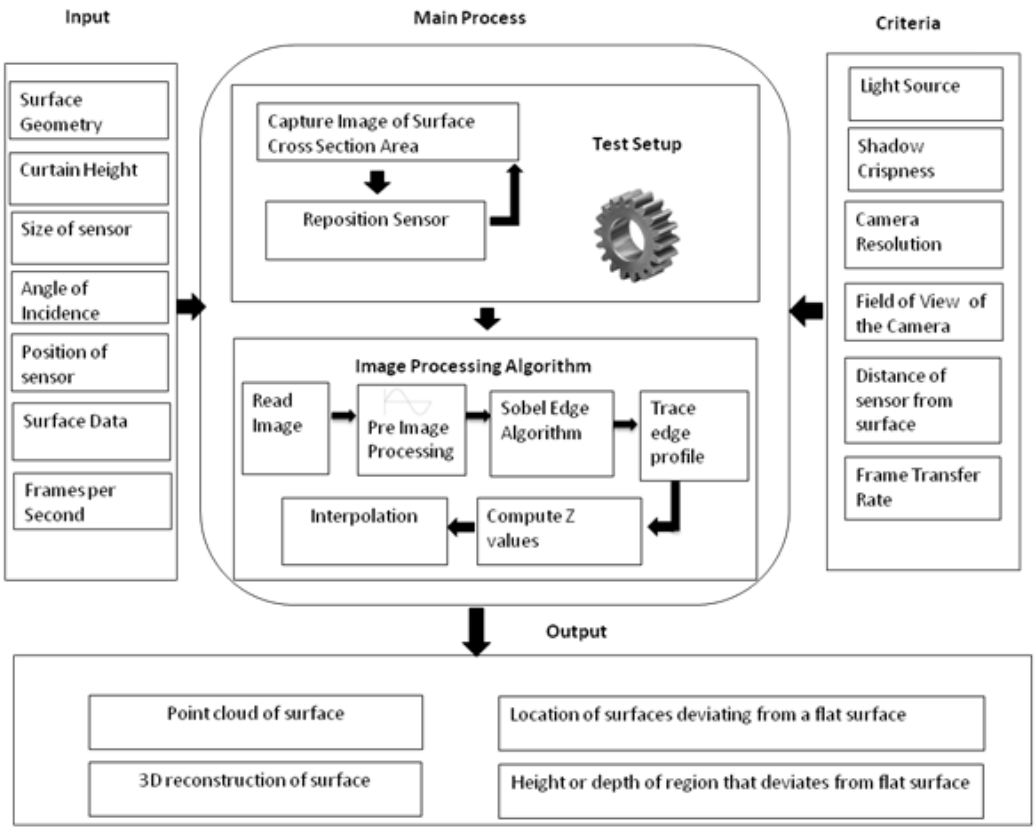

Figure 3.4: Proposed Methodology

3.3.1 Test Setup

Test setup in the scope of this research refers to the process of capturing information corresponding to a cross section area of the surface being evaluated. This information comprises of two segments, namely: 1) An image of the shadow profile over the surface cross section; and 2) The current location of the sensor.
The shadow profile is captured as an image from an overhead camera. Having the information regarding the location of the sensor, multiple images of the shadow profile can be used to reconstruct the surface profile.

A 3DS Max, virtual setup was established to test the proposed method. The drywall surface is modeled as a rectangular slab. Surface irregularities such as elevated bumps and depressions are also modeled into the surface. At the time of modeling the surface, parameters of the surface irregularities such as the height of elevation or the depth of a depression is known. This information is vital for validating the outputs obtained. The virtual setup established for the purpose of data collection is illustrated in Figure 3.5.

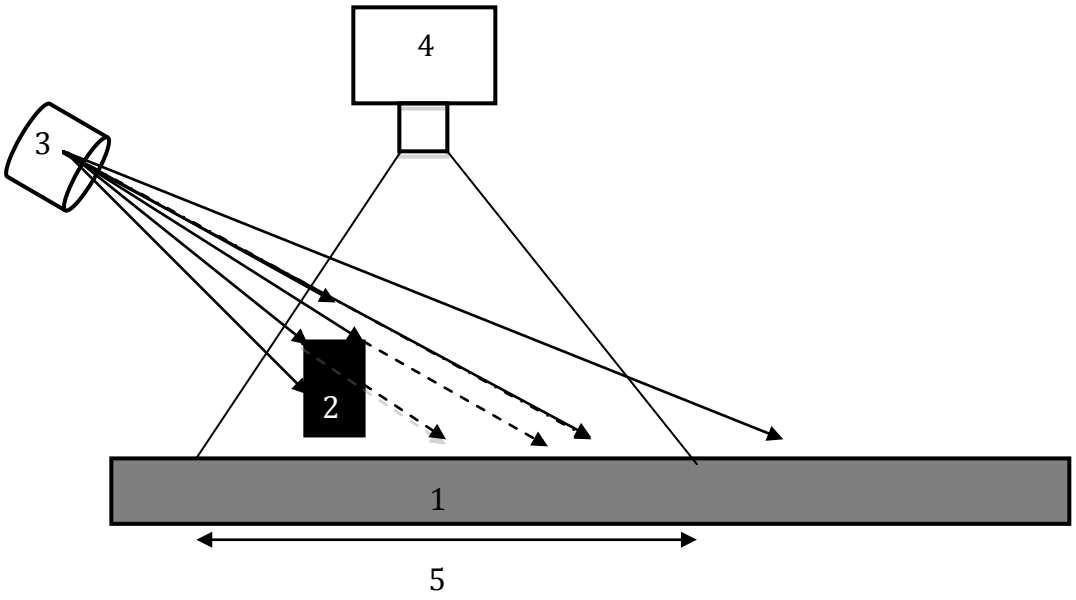

Figure 3.5: General schematic of proposed setup

The setup illustrated in Figure 3.5 comprises of the dry wall surface (1), a curtain to cast a straight edge shadow onto the surface (2), a light source (3), and a charge coupled device camera (4) to capture the shadow profile. The field of view of the overhead camera is denoted by region 5. The light source is modeled as a directional light source. The light is incident on the surface at an angle of 45^{o}. A straight edge shadow is cast upon the surface by a curtain, which is modeled as a rectangular slab of 2 cm height. A distance of 2 cm was maintained between the surface and the curtain. In practice this is done so as to assure that the curtain does not come in contact with the surface, thereby preventing any damage. The shadow cast by the curtain was captured as a frame through the overhead camera, which was aligned perpendicular to the surface and the curtain. Each frame represents one cross section of the surface. In order to capture all sections of the surface, the

setup comprising of the light source, curtain, and the camera is moved, and images of the other cross sections of the surface are taken. The base simulation model developed for the research is shown in Figure 3.6.

Figure 3.6: 3D Simulation modeled generated

Before modeling the surface, it is important to have an understanding of how the drywall surface appears prior to the sanding process. Depressions in the surface such as electrical sockets and nail holes are a common occurrence. An example of this is shown in Figure 3.7.

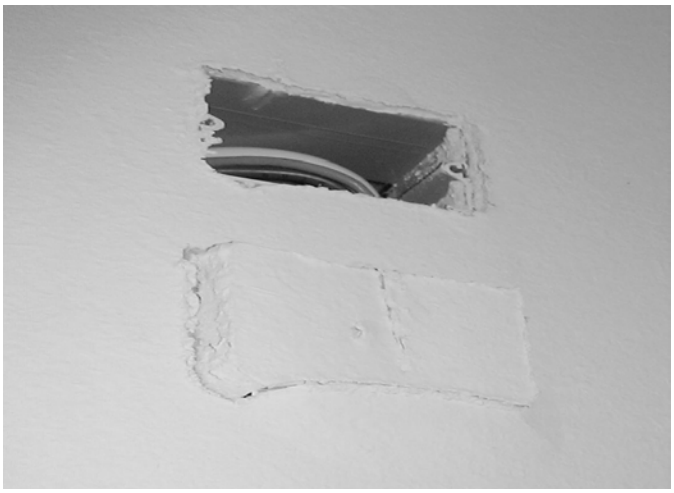

Figure 3.7: Dry Wall surface with an electric socket hole and mudded area

An idea of what the surface would resemble following the application of the joint compound is shown in Figure 3.8. Though the surface is skimmed with a taping knife, surface irregularities are still prominent.

Figure 3.8: Surface after application of joint compound.

As can be seen in Figure 3.7 and Figure 3.8, the base profile of a surface can be categorized into three types, namely: 1) Region of flatness; 2) Region that is elevated above normal flatness, such as surfaces with joint compound applied to it; and 3) Depressions in the surface, such as electric socket and nail holes.

The modeled surfaces have to emulate the categories mentioned above. Figure 3.9 below give a representation of how the surfaces were modeled in the virtual setup.

(a) Flat surface

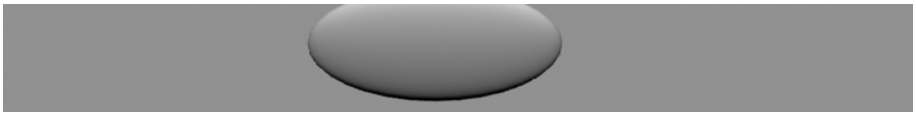

(b) Smooth Bump modeled on the surface

(c)Electric socket cut into the surface

(d) Nail hole in the surface

Figure 3.9: Examples of how surfaces were modeled in a virtual setup

3.3.2 Image Processing Algorithm

This section discusses the image processing algorithm of the proposed methodology. The output of the test setup comprises of a set of snapshots of the shadow profile over the surface. The images are then processed using the digital image-processing algorithm depicted in Figure 3.10.

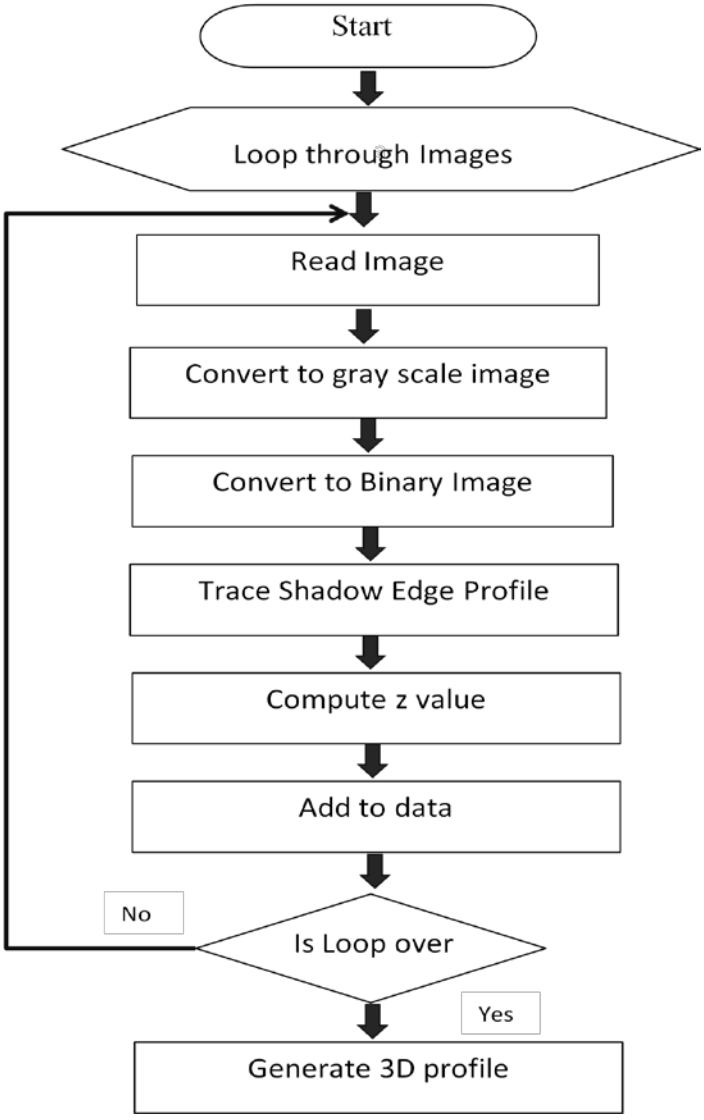

Figure 3.10: High level flowchart of computational logic

For digital image processing to be carried out on any image, the image should be in a form that can be suitably read by the program. Each image is defined by a set of pixels, which are basically rectangular cells. A collection of such cells constitutes an image. Each pixel is associated with a value known as the pixel value, which contains information pertaining to the color of the pixel. For color images that follow the RGB color space, pixel values are associated with three vectors, which represent the red, green and blue values of the pixel. In the case of

a grayscale image, this pixel value ranges from 0 to 255, which denotes the intensity of luminance. A value of 0 represents the color black, while a value of 255 is associated with the color white. Binary images contain either a value of 0 or 1 as their pixel value. The value 0 in this case also represents the color black and 1 represent the color white. The images outputted from the simulation model are characterized by the RGB color space. The RGB color format is an additive process, comprising of the three primary colors: red, green, and blue. In this process, the three colors are mixed to provide a wide range across the color spectrum. The first step of the algorithm involves reading the first sample image into the program workspace. The image is stored as a multidimensional matrix, comprising of red, green, and blue values, which correspond to a pixel value.

The image matrix then undergoes a set of preprocessing algorithms. The first preprocessing operation carried out on it is the grayscale scale conversion. Following this operation a new image matrix is created. This matrix comprises of values between 0 and 255. The second set of preprocessing algorithms converts the grayscale image into a binary image based on a threshold method. In this method, a threshold value is established. Each pixel is checked across the threshold value. If the pixel value is below the threshold, it is reset to 0, and for values greater than or equal to the threshold, the pixel value is set to 1. The end result of the binary operation results in an image matrix comprising of the binary values of 0 and 1.

The next step of the image processing algorithm requires tracing the edges in the image. The Sobel edge detection is used to trace the edges in the image. After the binary image has been processed with the edge algorithm, a matrix of binary values is obtained. An edge pixel is represented by a value of 1. The remaining pixels carry a value of 0. Once the edges have been traced, the x and y coordinates corresponding to the pixels on the edge are obtained. Using these values the corresponding z value is computed using the equations discussed in the latter part of this chapter.

3.3.2.1 Sobel Edge Algorithm

An edge in an image is defined as those areas that exhibit a strong change in luminous intensity, as it progresses from one pixel to another. Edge detection is a process that maintains the skeletal structure of an image, while filtering out the remaining portions of the image, which may not have any relevance in the data processing. Though there are various algorithms associated with edge detection, they can be classified into two categories namely, “Gradient based” and “Laplacian based” methods. In the gradient method edges are detected by locating pixels between which the jump in intensity is maximum. In the Laplacian method, edges are found at the zero crossing of the second directional derivative (Vincent and Folorunso, 2009).

A gradient is basically a vector, whose components determine the changes in the value of a pixel in the x and y directions, satisfying Equations (1) and (2) respectively (Vincent and Folorunso, 2009).

$$\Delta x = \left\{\frac{f((x+dx),y) - f(x,y)}{dx}\right\} \quad (1)$$

$$\Delta y = \left\{\frac{f(x,(y+dy) - f(x,y)}{dy}\right\} \quad (2)$$

Where;

Δx= gradient vector along the *x* direction

Δy= gradient vector along the *y* direction

dx = measurement of the distance along the *x* axis as shown in Figure 3.11(a)

dy = measurement of the distance along the *y* axis as shown in Figure 3.11(b).

(a) (b) (c)

Figure 3.11: Examples of gradient along the *x* direction (a) , *y* direction (b) and in both directions(c)

The strength of the edge (*M*) is determined by the magnitude of the gradient, which is calculated using Equation (3)

$$M = \sqrt{\Delta x^2 + \Delta y^2} \quad (3)$$

The Sobel method belongs to the "gradient filter" family of edge detection algorithms. The Sobel edge algorithm incorporates the use of the Sobel operators

(*Gx* and *Gy)*, which is a pair of 3 x 3 convolution kernels, which satisfy Equations (4) and (5).

$$Gx = \begin{bmatrix} -1 & 0 & 1 \\ -2 & 0 & 2 \\ -1 & 0 & 1 \end{bmatrix} \quad (4)$$

$$Gy = \begin{bmatrix} -1 & -2 & -1 \\ 0 & 0 & 0 \\ 1 & 2 & 1 \end{bmatrix} \quad (5)$$

Using these two operators, the gradient of the image intensity in each orientation is calculated by a process of convolution satisfying Equations (6) and (7).

$$\Delta x = \begin{bmatrix} -1 & 0 & +1 \\ -2 & 0 & +2 \\ -1 & 0 & +1 \end{bmatrix} * I \quad (6)$$

$$\Delta y = \begin{bmatrix} -1 & -2 & -1 \\ 0 & 0 & 0 \\ +1 & +2 & +1 \end{bmatrix} * I \quad (7)$$

where,

I = Image matrix

Δx= Matrix containing horizontal derivative approximations

Δy= Matrix containing vertical derivative approximations

If the intensity of the image is to be plotted as a function of the position, a signal is plotted as shown in Figure 3.12.

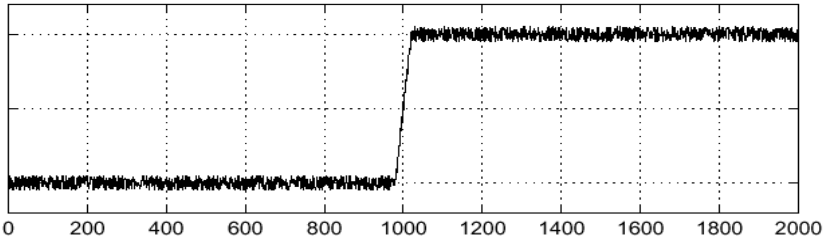

Figure 3.12: One-dimensional representation of an edge

Figure 3.13 gives a representation of the operations that constitute the edge algorithm.

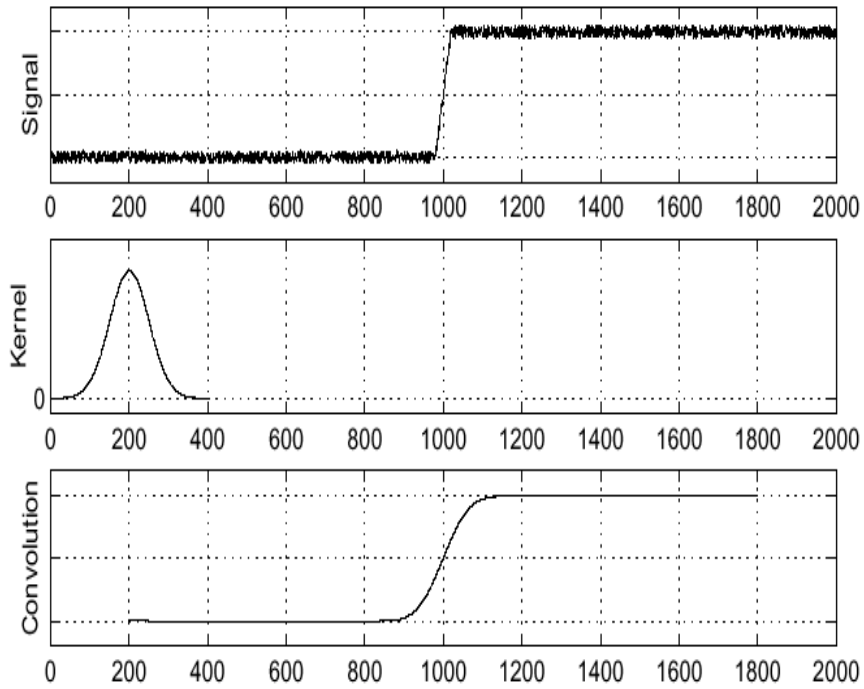

Figure 3.13: Convolution Operation of Sobel Edge Algorithm

In regions where the intensity changes, there will be a peak in the first directional derivative. An edge location is typically identified as peaks in the first directional derivative. This is illustrated in Figure 3.14.

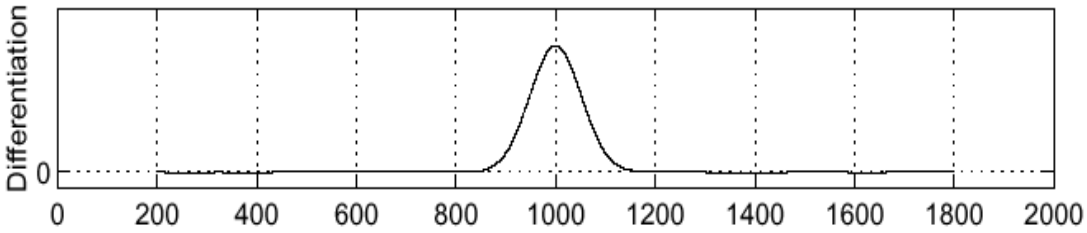

Figure 3.14: First directional derivative of convoluted signal.

Consider an image of a chessboard, as shown in Figure 3.15; the image exhibits sharp jumps in intensity, as it progresses from one square to another.

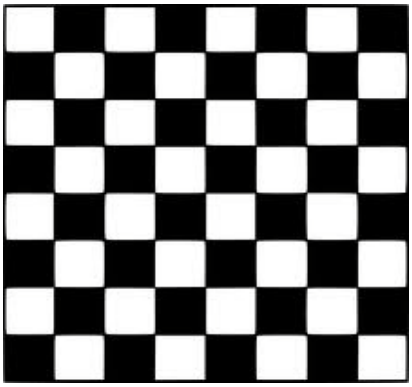

Figure 3.15: Original chessboard image

The objective of the edge algorithm is to trace the edges present in Figure 3.15; these edges are traced along the regions where the intensity change is maximum, such as the bridge between a black and white square. The result of the Sobel edge algorithm is shown in Figure 3.16.

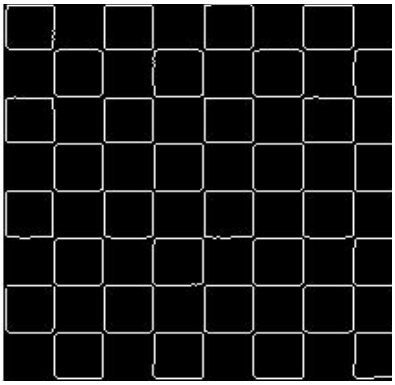

Figure 3.16: Result of applying the Sobel edge algorithm to Figure 3.15.

The image processing algorithm in this research has been programmed using the digital image processing toolkit, which is present in MATLAB.

3.3.2.2 3D Surface Reconstruction

This section describes the basic principles associated with reconstruction of a 3D profile of a surface. Once an object's edge has been detected, each pixel value is then fed into a set of equations (which will be explained in the following chapter). The result of this computational logic is a set of x, y, and z coordinates, which denote a point cloud of the surface profile. A point cloud is basically defined as a set of vertices in a 3D coordinate system. Reconstruction of a surface profile from a point cloud can be achieved through linear interpolation algorithm. Interpolation is a concept that is used to estimate the value at unknown points. For example, if two data points (x_0, y_0) and (x_1, y_1) are previously known, any unknown value within the interval can be determined through linear interpolation. In linear interpolation, for an interval, $0 < k < 1$, the value of the point (x_k, y_k) is the value that satisfies the equation of the line passing through (x_0, y_0) and (x_1, y_1). This is illustrated in the Figure 3.17.

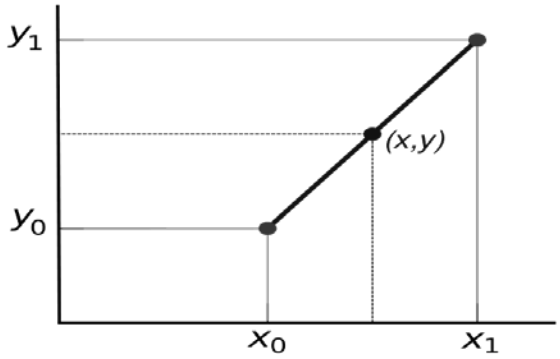

Figure 3.17: Interpolation on a 2D plane

Similarly, in the case of an image, interpolation is used to determine an unknown pixel's value on the basis of its surrounding pixels. Consider the example of an image, as shown in Figure 3.18(a); scaling the image upwards would result in

unknown pixel values. In the absence of these values the scaled image loses its clarity, when compared with the original image. These unknown pixel values are determined using linear interpolation based on the surrounding pixel values. The effect of interpolation on a 2 D image is represented in Figure 3.18.

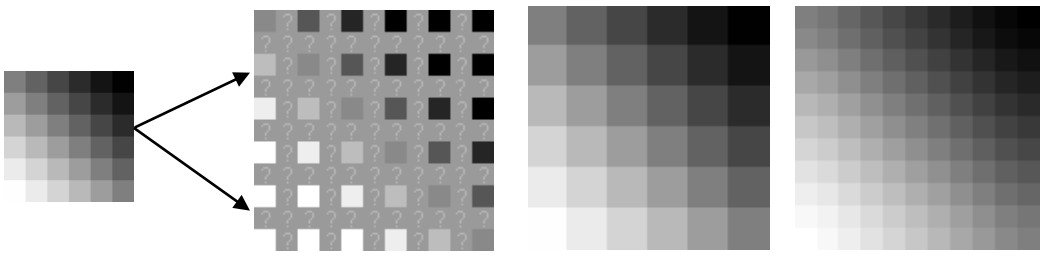

(a) Original Image (b) Scaled Image (c) Without Interpolation (d) With Interpolation

Figure 3.18: Interpolation on 2D image

3.3.3 Algorithm for Modeling a Flat Surface

This section looks at the mathematical set of algorithms which correspond to the shadow profiling of a flat surface. The algorithms presented in this section constitute the basis for applying shadow profilometry on a flat surface as illustrated in the Figures 3.19 and 3.20.

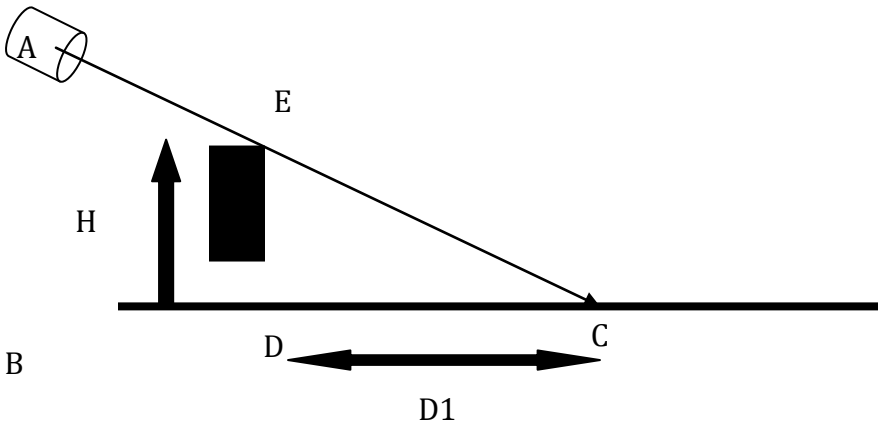

Figure 3.19: Modeling a flat surface

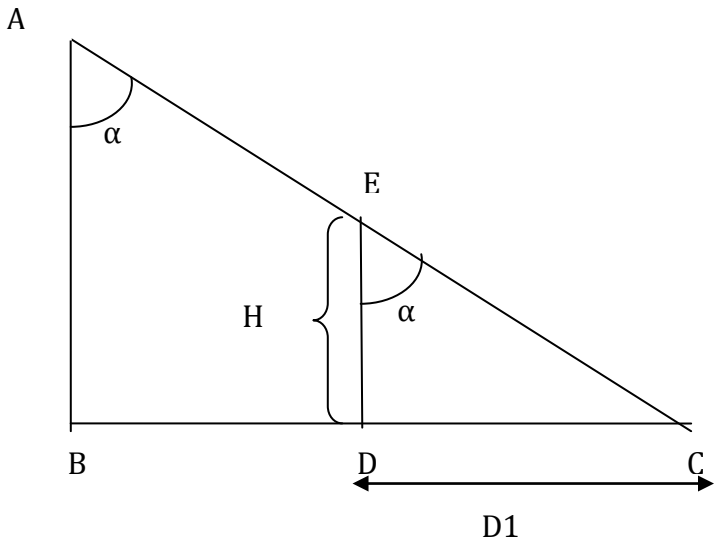

Figure 3.20: Geometric representation of Figure 3.19.

Figure 3.20 represents the geometric representation of Figure 3.19. The shadow profiling technique can be geometrically represented by two right angled triangles shown in Figure 3.20, namely,Δ ABC and ΔEDC. The line AC represents the direction of the light ray. AB represents the height of the light source from the surface. ED represents the height of the curtain, as measured from the top of the surface. This height is inclusive of the region of separation between the surface and the curtain. The line DC covers the region where the shadow is formed. The objective of the set of equations described here is to calculate the distance from the curtain at which the shadow edge is formed.

The light source is incident at an angle of α, which is denoted by ∠BAC. Since the curtain is placed perpendicular to the surface, AB and ED are parallel to each other; hence, as a result of alternate angles (α), satisfying Equation (8).

$$\angle BAC = \angle DEC \quad (8)$$

Let us denote the value of ED as H, and the distance at which the shadow edge is formed as D1, which can be calculated satisfying Equation (10)

In Δ EDC

$$\tan \alpha = \frac{DC}{ED} = \frac{D1}{H} \quad (9)$$

$$\boxed{D1 = H * tan\ \alpha} \quad (10)$$

When the surface is flat, the distance at which the shadow edge is formed, is dependent on the height of the curtain and the incident angle of the light, as shown in Equation 10. The knowledge of the distance at which a shadow is formed on flat surface, is important while dealing with irregular surfaces. The height or depth of a region that deviates from a flat surface is determined by evaluating the distance of the shadow edge, against the value that is calculated satisfying Equation (10).

For instance , for an angle of incidence, α, of 45^o,

$$tan\ \alpha = 1 \quad (11)$$

Hence from Equation 9,

$$D1 = H \quad (12)$$

At an incidence angle of 45^o, the distance at which a shadow edge is formed is equal to the height of the curtain.

3.3.4 Algorithm for Determining Deviations in Elevations in the Surface

Generally, surfaces that have been filled with a joint compound exhibit an elevation in their surface profile. The objective of the set of algorithms mentioned below is to obtain the height (*X*) of the elevated area from the regular surface, as illustrated in Figures (3.21) and (3.22).

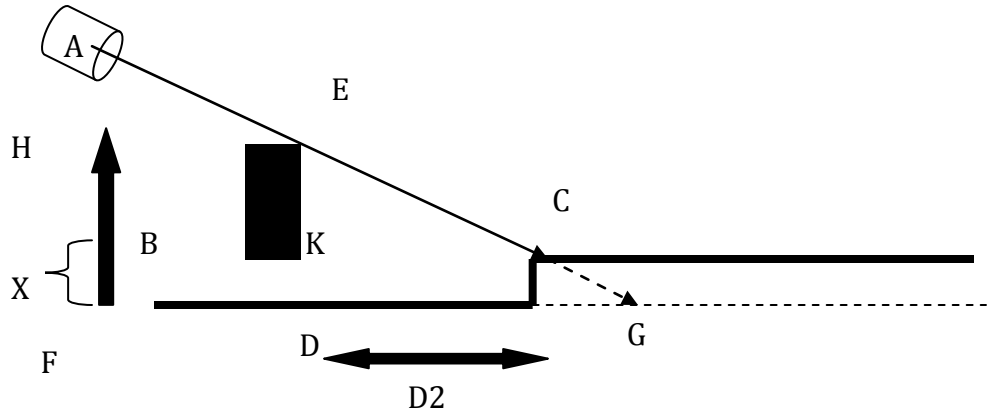

Figure 3.21: Elevated surface modeling

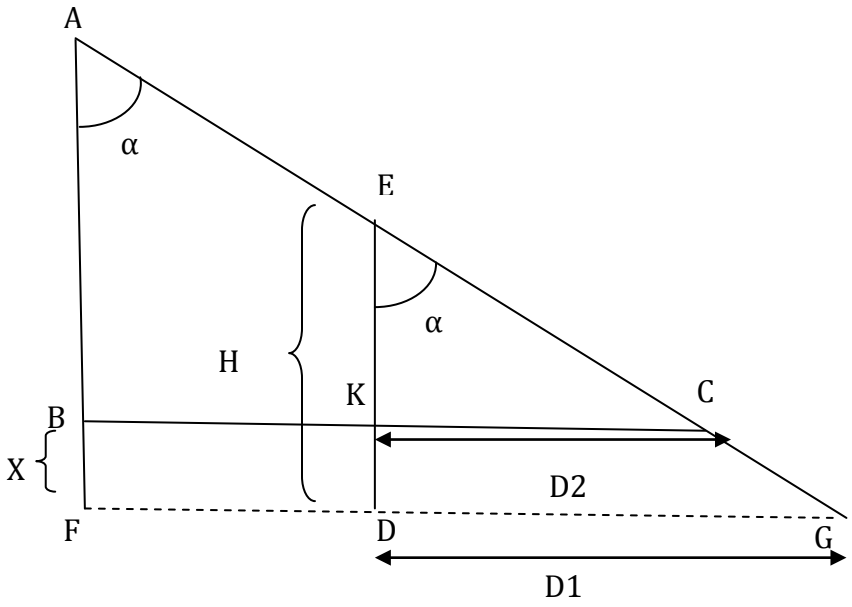

Figure 3.22: Geometric representation of Figure 3.21.

The line AC represents the direction of the light ray. AF represents the height of the light source from the surface, and ED represents the height of the curtain from the surface. This height is inclusive of the region of separation between the surface and the curtain. The region where the shadow is formed is denoted by line KC. DG represents the area where the shadow edge would have been formed, had the surface been flat. The light source is incident at an angle of α, which is denoted by ∠BAC. Since the curtain is placed perpendicular to the surface, AB and ED are parallel to each other; hence, as a result of alternate angles (α), satisfying Equation (13).

$$\angle \text{ BAC} = \angle \text{DEC} \tag{13}$$

Let ED be denoted as H. The distance at which the shadow edge is formed, KC, is denoted as D2. The height of the deviation BF is taken as X.

Hence,

$$EK = H - X \tag{14}$$

Based on Δ EKC $tan\ \alpha$, can be calculated satisfying Equation (15).

$$tan\ \alpha = \frac{KC}{EK} \tag{15}$$

By substitution the Deviation(X) can be calculated satisfying Equation (16).

$$tan\ \alpha = \frac{D2}{H - X} \tag{16}$$

$$D2 = (H - X) * tan\ \alpha \tag{17}$$

$$\boxed{X = \frac{(H * \tan \alpha) - D2}{\tan \alpha}} \tag{18}$$

From Equation (9) we get,

$$D1 = H * tan\ \alpha$$

where;

D1 = Distance of the shadow edge on flat surface.

Further substitutions from Equation (9) , the deviation (*X*) can be calculated satisfying Equation (19).

$$\boxed{X = \frac{D1 - D2}{\tan \alpha}} \qquad (19)$$

3.3.5 Algorithm for Determining Deviations in Depressions in the Surface

A drywall surface may contain depressions such as holes caused by nails or a cut out for electric sockets. The objective of the set of algorithms mentioned below is to obtain the depth (*X*) of the elevated area from the regular surface, as illustrated in figures (3.23) and (3.24).

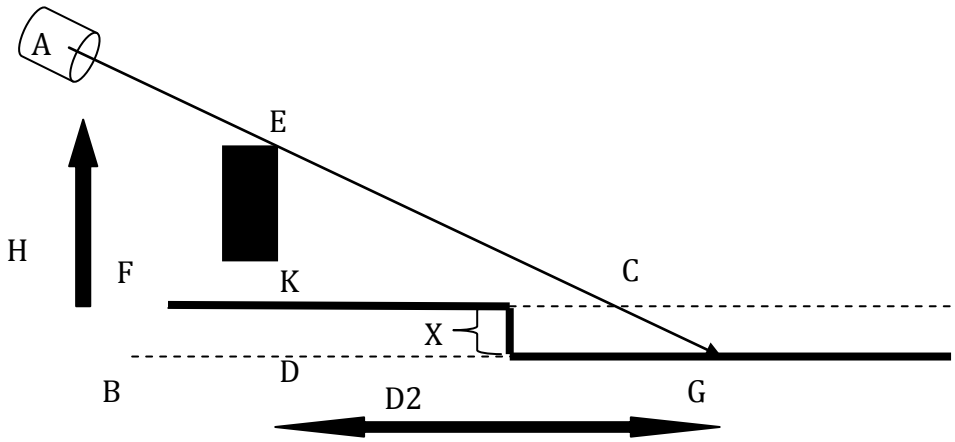

Figure 3.23: Depression in surface modeling

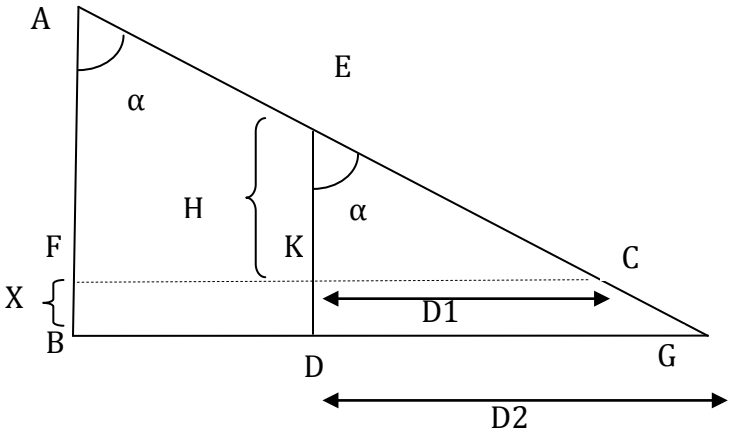

Figure 3.24: Geometric representation of Figure 3.23.

The line AC represents the direction of the light ray. AF represents the height of the light source from the surface, and EK represents the height of the curtain from the surface. This height is inclusive of the region of separation between the surface and the curtain. DG represents the region where the shadow is formed. KC represents the area where the shadow edge would have been formed had the surface been flat. The light source is incident at an angle of α, which is denoted by ∠BAC. Since the curtain is placed perpendicular to the surface, AB and EK are parallel to each other; hence, as a result of alternate angles (α), satisfying Equation (20).

$$\angle \text{ BAC} = \angle \text{KEC} \qquad (20)$$

Let EK be denoted as H. The distance at which the shadow edge is formed, DG, is denoted as D2. The depth of the depression BF is taken as X.

Hence,

$$ED = H + X \qquad (21)$$

Based on Δ EDG $tan\ \alpha$, can be calculated satisfying Equation (22).

$$\tan\alpha = \frac{DG}{ED} \quad (22)$$

By substitution the Deviation(X) can be calculated satisfying Equation (25).

$$\tan\alpha = \frac{D2}{(H+X)} \quad (23)$$

$$D2 = (H+X) * \tan\alpha \quad (24)$$

$$\boxed{X = \frac{(D2 - (H * \tan\alpha))}{\tan\alpha}} \quad (25)$$

From Equation (9) we get,

$$D1 = H * tan\ \alpha$$

where,

D1 = Distance of the shadow edge on flat surface.

Further substitutions from Equation (9) , the deviation (X) can be calculated satisfying Equation (26).

$$\boxed{X = \frac{(D2 - D1)}{\tan\alpha}} \quad (26)$$

Chapter 4: Implementation of Proposed Methodology

4.1 Case Studies

This section evaluates different case studies and discusses the results of each. The cases considered in this section are as follows

1. Regular flat surface.
2. Surface with elevations.
3. Surface with electric socket-like depressions.
4. Surface with a nail hole.

The height and depth of a surface irregularity can be determined using Equations (19) and (26), which are,

$$Equation\ (19): Height\ of\ surface\ irregularity = \frac{D1 - D2}{\tan \alpha}$$

$$Equation\ (26): Depth\ of\ surface\ irregularity = \frac{D2 - D1}{\tan \alpha}$$

where;

D1 = distance of shadow edge on a flat surface.

D2 = distance of shadow edge on irregular profile.

As observed, Equations (19) and (26), differ only in whether they are a positive or a negative value. The magnitudes of both equations are the same. When using Equation (19) during the implementation, a positive result would identify the

irregularity as an elevated region, while a negative result would signify a depression in the region. If the surface under consideration is flat, then

$$D2 = D1 \qquad (27)$$

By substitution of Equation (27), the result of Equation (20) would be 0, which denotes the absence of surface deviations.

4.1.1 Flat Surface

In this case study, the surface is considered to be free from any defect. In other words, it is a flat smooth surface. The base model of the case study is shown in Figure 4.1

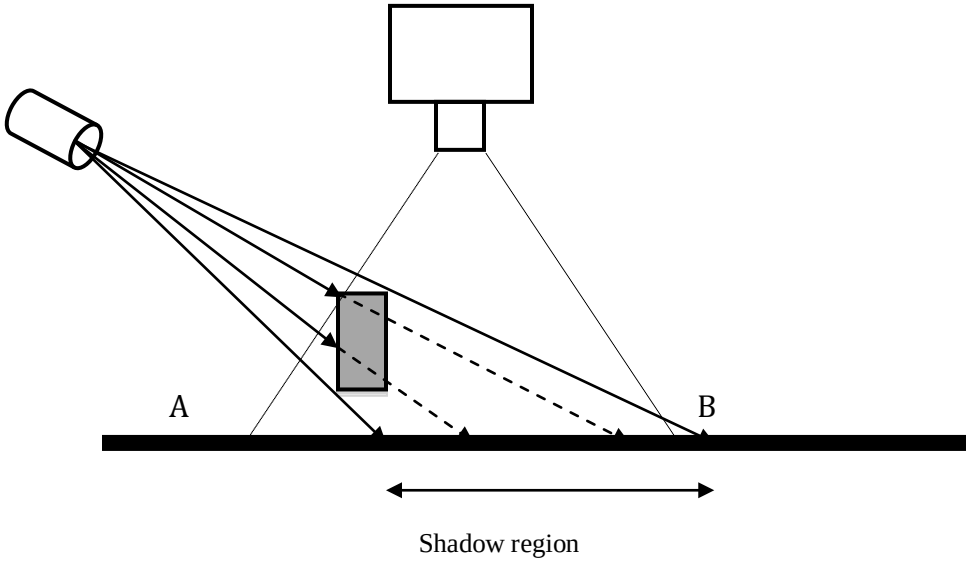

Figure 4.1: Base model for flat surface simulation

The field of view AB, shown in Figure 4.1, is the viewable region of the overhead camera. Figure 4.2 provides a top view of the surface, which is taken from the

perspective of the camera above. The black region in the image represents the shadow formed by the curtain.

Figure 4.2: Top view from camera perspective

Snapshots of the surface are taken from Autodesk 3DS Max. The camera captures the top view of the model. At a given point in time, only a particular cross section area of the surface can be mapped. The surface is broken into sections. Each section is captured as a snapshot and processed individually. The result of each section is then compiled together to reconstruct the 3D profile of the entire surface. Each image goes through a preprocessing algorithm, which isolates the region of interest, in this case the edge of the shadow profile. Following preprocessing, the Sobel edge detection algorithm is performed on the image. The result of the edge algorithm is shown in Figure 4.3.

Figure 4.3: Edge profile of sampled image

Each point on the edge is evaluated, and the result is stored into the 3D matrix, which comprises of the *x*, *y*, and *z* coordinates of each point. Having this data available, a point cloud is generated as shown in the Figure 4.4.

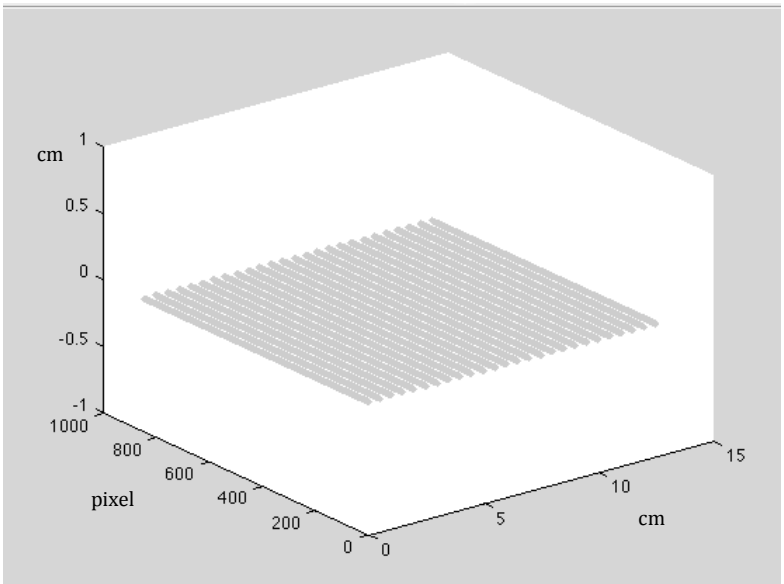

Figure 4.4: Point cloud of flat surface

Surface reconstruction from the point cloud is done using the interpolation algorithm, which is present in MATLAB's toolkit. The interpolation algorithm is used to fit a surface onto the points that have been computed, as shown in Figure 4.5.

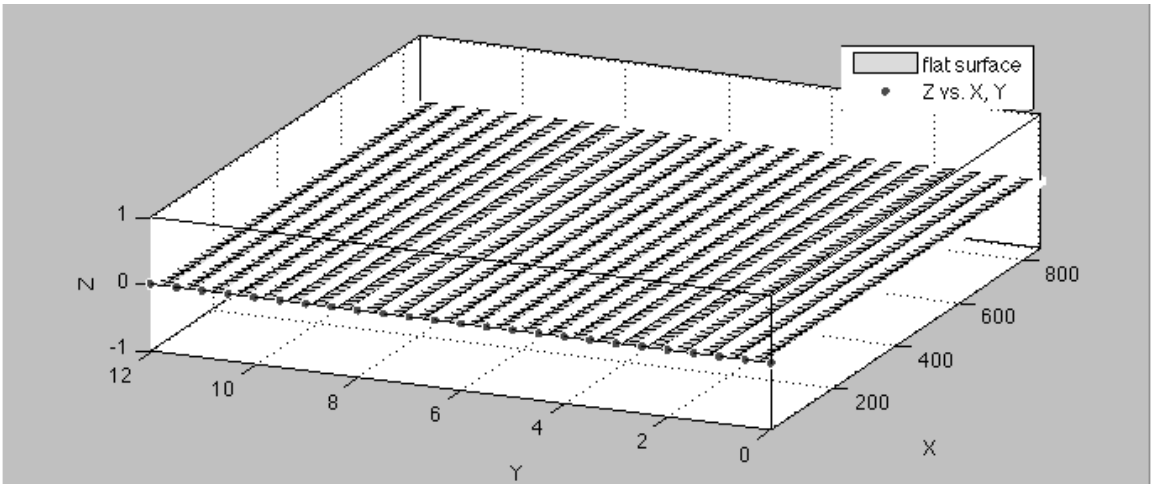

Figure 4.5: 3D reconstruction of flat surface profile

As can be seen from the Figure 4.5, each point on the surface has a 0 value on the *z* axis. Validation is carried across the base model, which was modeled as a flat surface with no irregularities in its profile. The computed model was found to have no deviation from the original surface.

4.1.2 Surface with elevation

A curved elevated surface is most common, prior to drywall sanding. The surface profile gradually ascends at regions where the joint compound has been applied. This surface profile was modeled using an elliptical curve. The maximum height of this region of elevation from the base of a flat surface was modeled as 1 cm. The aim of this case study is to reconstruct the 3D profile of this surface, and obtain the maximum (*z*) elevation through computation. The base model of an elevated curved surface is shown below in Figure 4.6

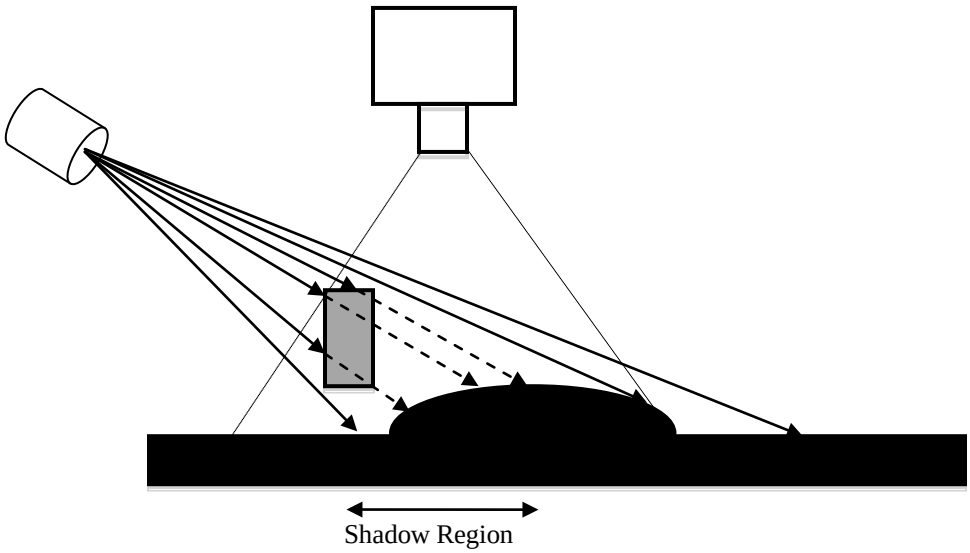

Figure 4.6: Base model for simulation of an elevated surface profile

As seen in the Figure 4.7, the shadow profile is a straight line over a flat surface; however, as the virtual setup progresses over the surface defect, the shadow profile deviates from a straight line, as can be seen in Figure 4.7.

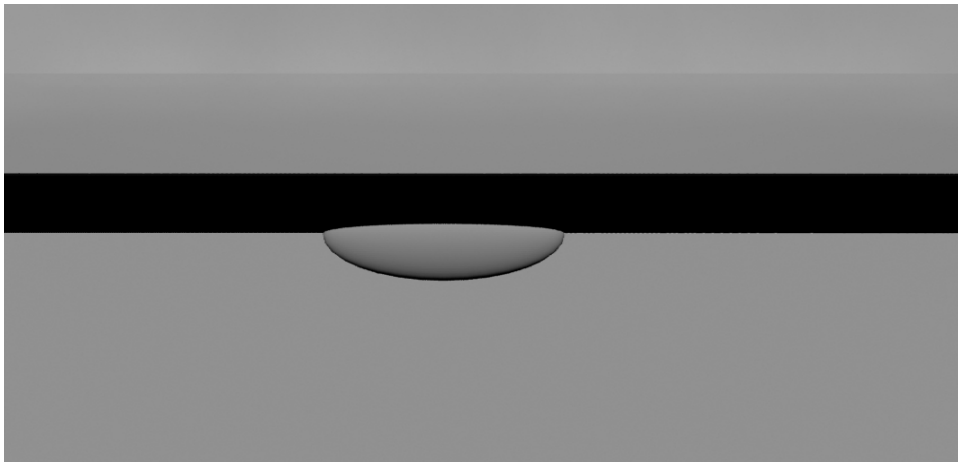

Figure 4.7: Elevated surface sample image

Note that in case of an elevation, the shadow edge follows the pattern that was explained in section 3.3.3.4. Applying the edge algorithm on this profile, has the following result as shown in Figure 4.8.

Figure 4.8: Edge profile of sampled image

Computation is carried out on all points forming the edge profile. The point cloud generation based on the computed values is shown below in Figure 4.9.

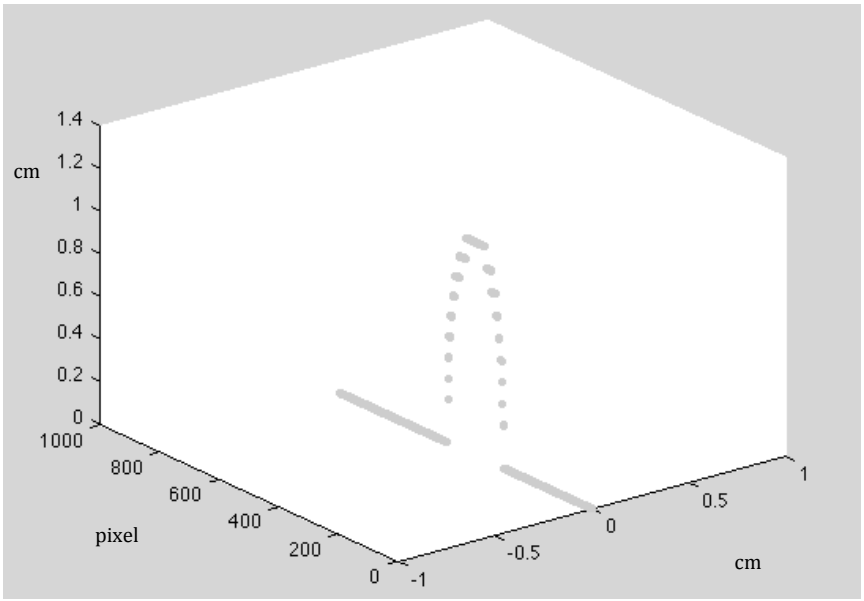

Figure 4.9: Point cloud of sampled image

The maximum height of the curved profile was found to reach the value 1 cm on the z axis. This corresponds to the maximum height in the base model. After

images corresponding to different sections of the surface have been processed, a point cloud is generated as shown in Figure 4.10.

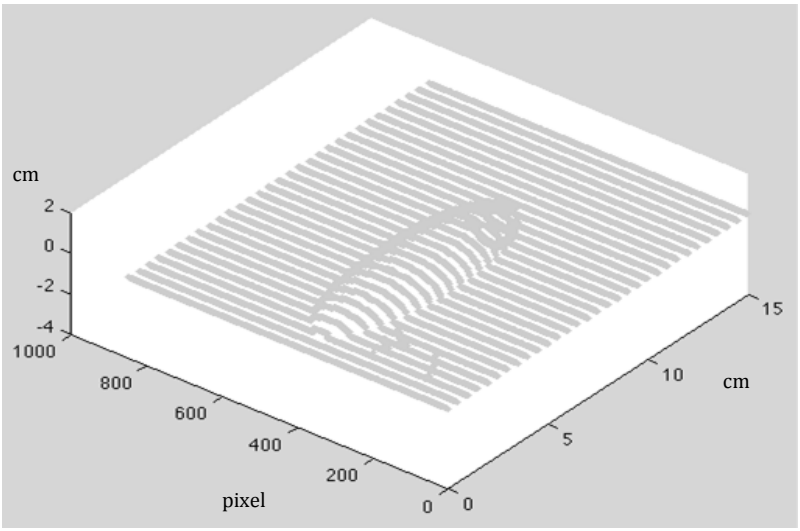

Figure 4.10: Point cloud of elevated surface

The three dimensional reconstruction is then carried out making, use of the MATLAB interpolation surface fitting tool. The result of this is shown in the figure below (Figure 4.11).

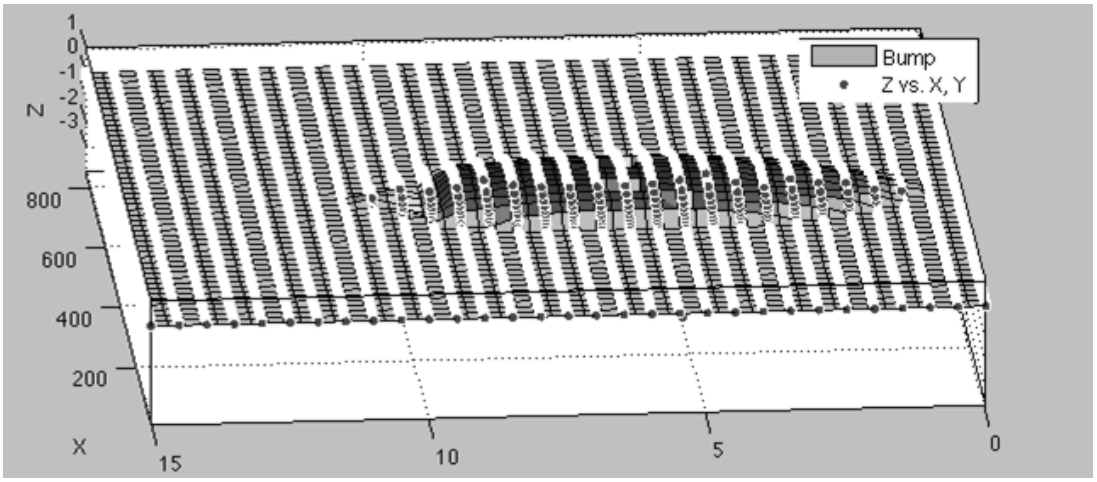

Figure 4.11: 3D reconstruction of elevated surface profile

The output was validated against the original data. Points corresponding to the point cloud are compared against the original points of the particular section in the base model. By comparing the results of different sections of the surface with the original data, the maximum, minimum, average error and standard deviation was determined as shown in Table 4.1

Table 4.1: Validation results of case 2

Maximum Error	:	0.1 cm
Minimum Error	:	0 cm
Average Error	:	0.04 cm
Standard Deviation	:	0.047

Apart from the shadow cast by the curtain, it was found that a secondary shadow was formed in some of the images. Owing to the nature of the surface profile, the elevated region would prevent light from reaching regions of lower elevation, hence creating a secondary shadow. The average error was found to be (0.04) cm, with a few points deviating with a maximum error of (0.1) cm.

4.1.3 Surface with an Electric Socket-like Depressions

Irregular surfaces not only comprise of elevations, but also depressions such as electric sockets. In this case study, the surface depression is modeled as a socket as shown in the Figure 4.12.

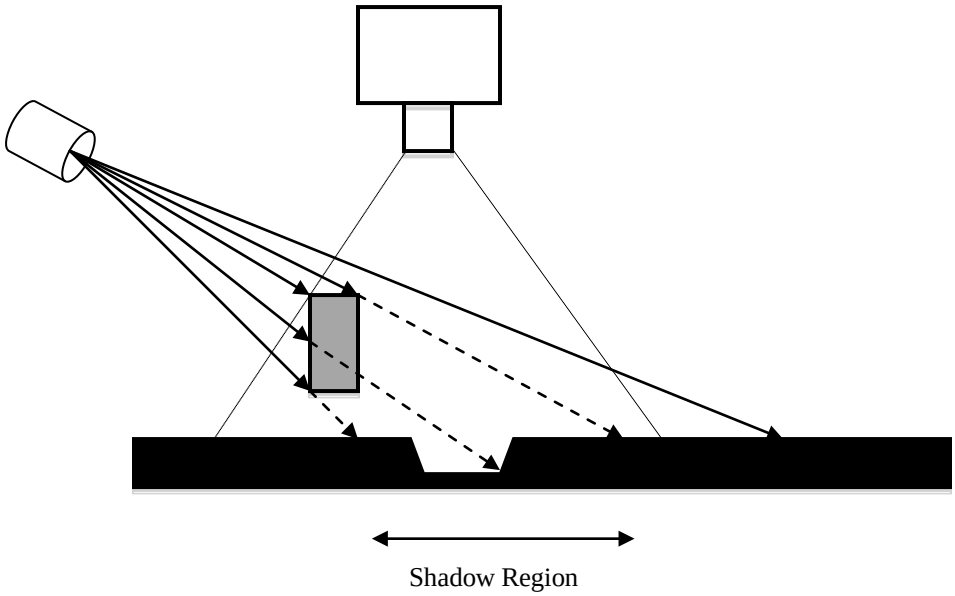

Figure 4.12: Base model of depression in the surface

The figure below represent the shadow profile as it progress over the socket.

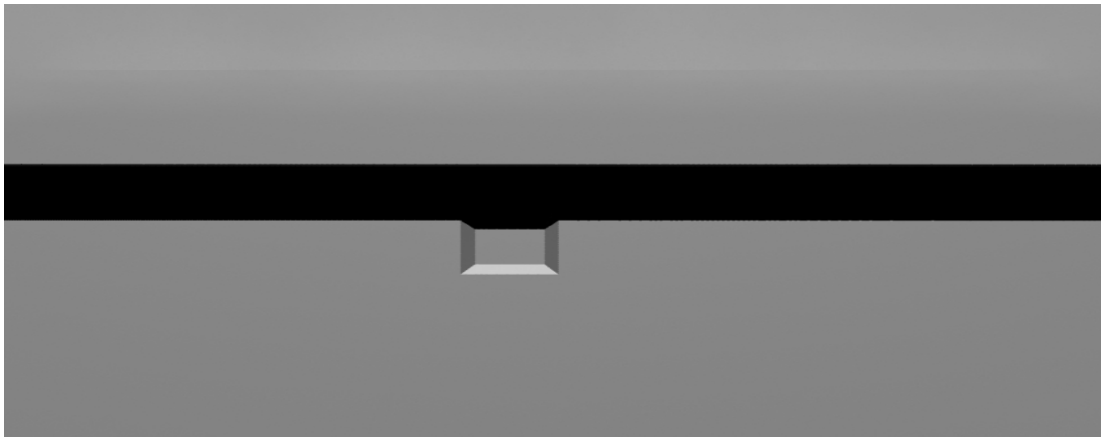

Figure 4.13: Sample image of depression in surface

The edge and point cloud profile of the image above is shown in Figure 4.14 and Figure 4.15, respectively.

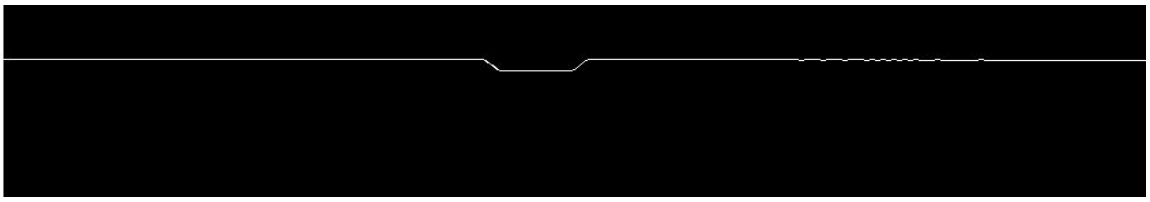

Figure 4.14: Edge profile of sampled image

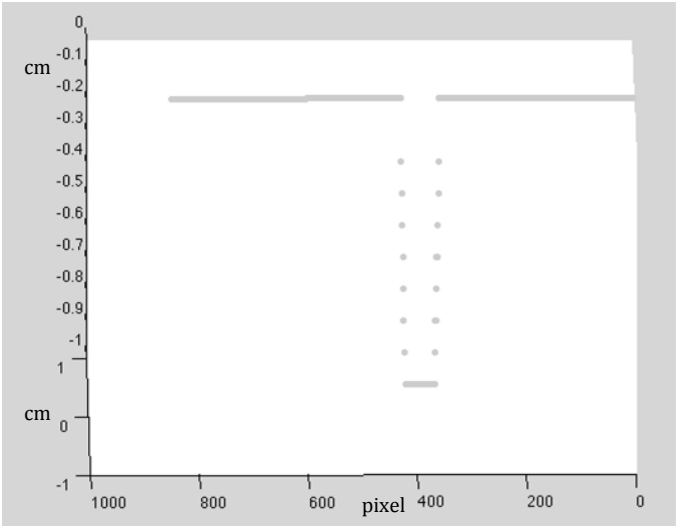

Figure 4.15: Point cloud of sampled image

The images are sampled over a given interval, and the 3D profile is constructed following the generation of the point cloud. The images below showcase the point cloud and reconstructed model (Figures 4.16 and 4.17).

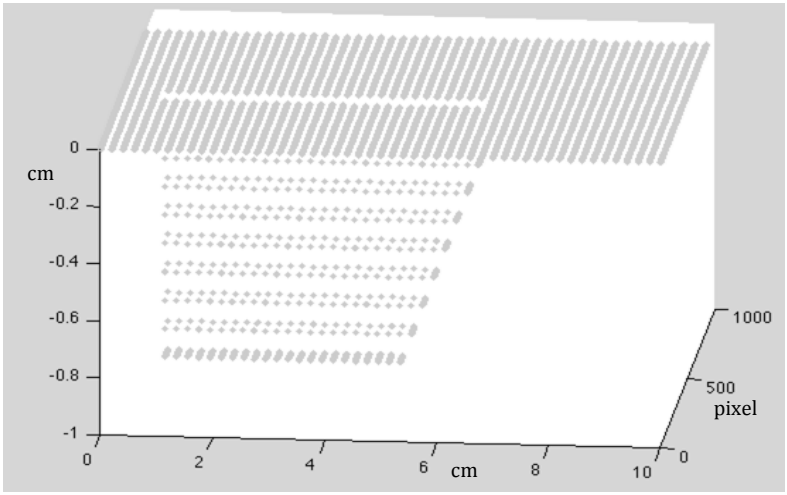

Figure 4.16: Point cloud of surface profile

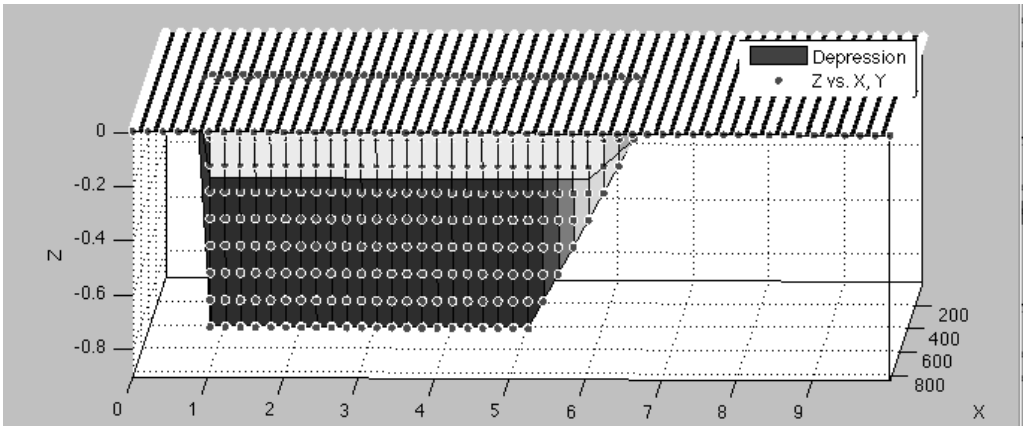

Figure 4.17: 3D reconstruction of depression in surface profile

Points corresponding to the point cloud are compared against the original points of the corresponding section in the base model. By comparing the results of different sections of the surface with the original data, the maximum, minimum, average error and standard deviation was determined as shown in Table 4.2.

Table 4.2: Validation results of case 3

Maximum Error	:	0.1 cm
Minimum Error	:	0 cm
Average Error	:	0.01 cm
Standard Deviation	:	0.03

The average error was found to be better in comparison with the results of case study 2. It was found that the shadow profile closely followed the surface topography, and only few points deviated from the original values.

4.1.4 Surface with a Nail Hole

Another defect that is a common occurrence in drywall is nail holes. Usually the nail holes are covered by the joint compound; however in the event that they have not been, the sensor should be able to profile the surface. Figure 4.18 represents a typical drywall nail hole.

Figure 4.18: Nails in drywall

The nail hole was modeled in the 3D model in a pattern similar to a cone. The outer perimeter of the hole was elevated above the surface level, while caving inwards towards the center. The base model of this case study is shown in Figure 4.19 and Figure 4.20.

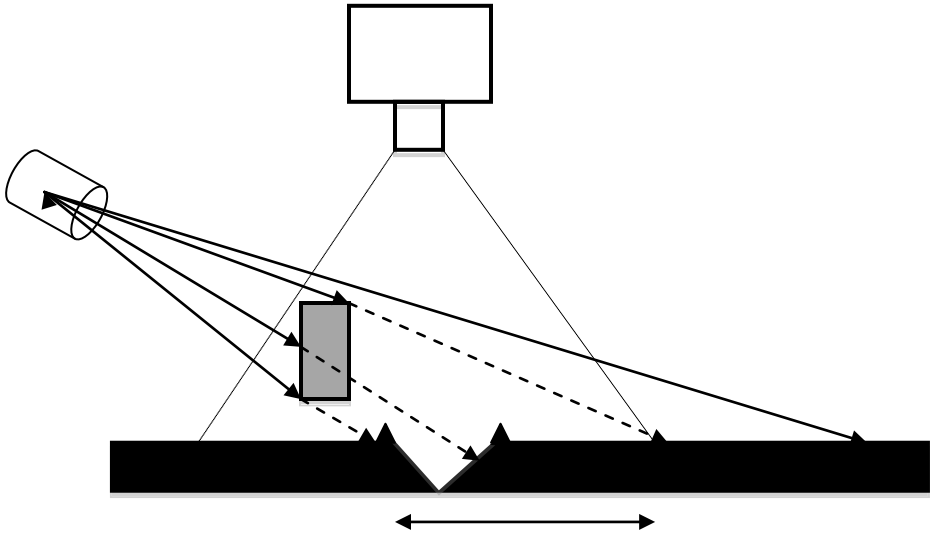

Figure 4.19: Base model of depression in the surface

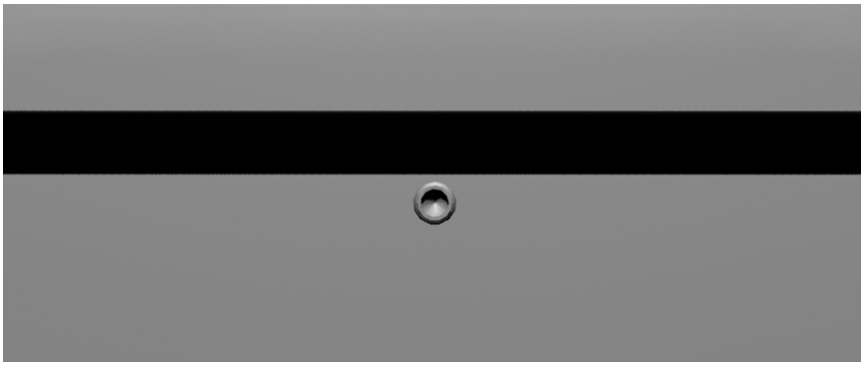

Figure 4.20: Simulated representation of nail holes

The surface under simulation consists of a mix of elevations and depressions. The shadow profile of the setup over the whole structure is shown in Figure 4.21.

Figure 4.21: Sample image of shadow over nail hole

The edge profile of the sampled image is given below in Figure 4.22.

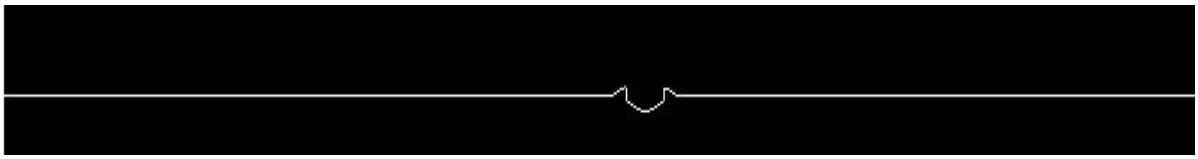

Figure 4.22: Edge profile of sampled image

The point cloud of the edge profile above gives a better understanding of how surface profiling is done. As can be seen above, some sections of the edge profile

are over the flat line, while others are below. The point cloud was generated of the above sample, and is shown in Figure 4.23.

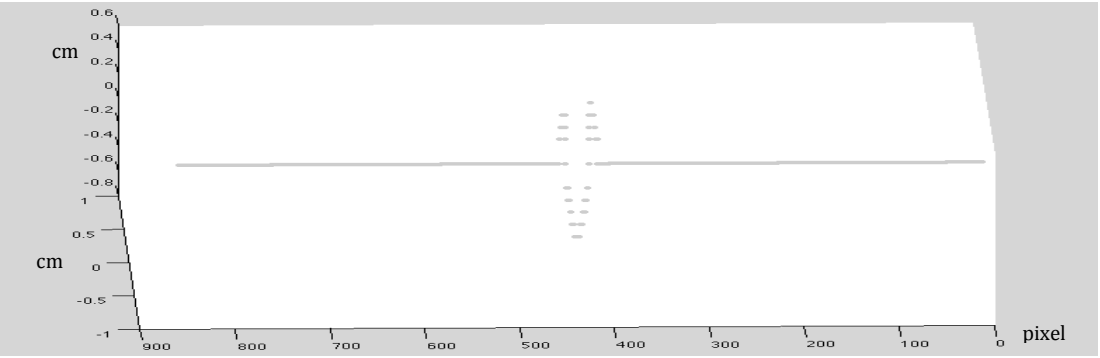

Figure 4.23: Point cloud of edge profile

Sampled over an interval, the point cloud was generated for the entire section of the hole. This is shown in the figure below (Figure 4.24).

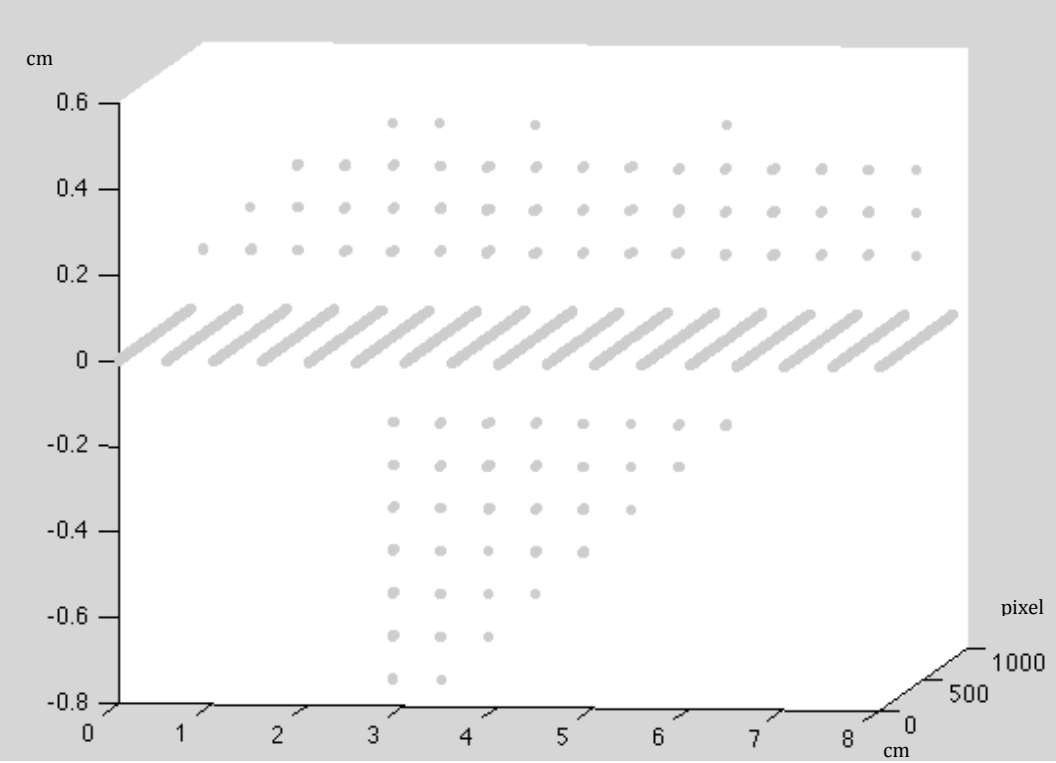

Figure 4.24: Point cloud of surface with nail hole

The 3D reconstruction of the surface is shown below in Figure 4.25.

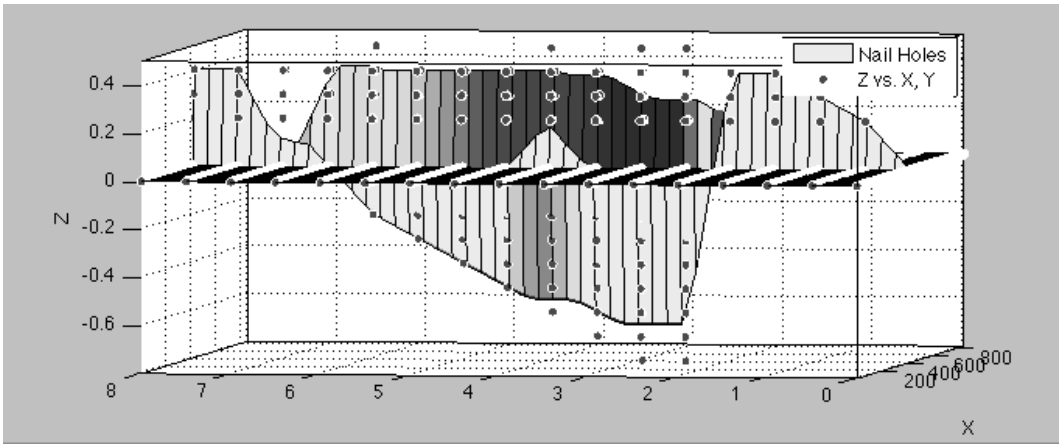

Figure 4.25: 3D reconstruction of surface

Points corresponding to the point cloud are compared against the original points of the corresponding section in the base model. By comparing the results of different sections of the surface with the original data, the maximum, minimum, average error and standard deviation was determined as shown in Table 4.3.

Table 4.3: Validation results of case 4

Maximum Error	:	0.3 cm
Minimum Error	:	0.1 cm
Average Error	:	0.02 cm
Standard Deviation	:	0.069

4.1.5 Surface with Narrow Depression

The surface of the drywall may also contain deep cracks in its surface which can be modeled as a narrow deep depression as shown in Figure 4.26.

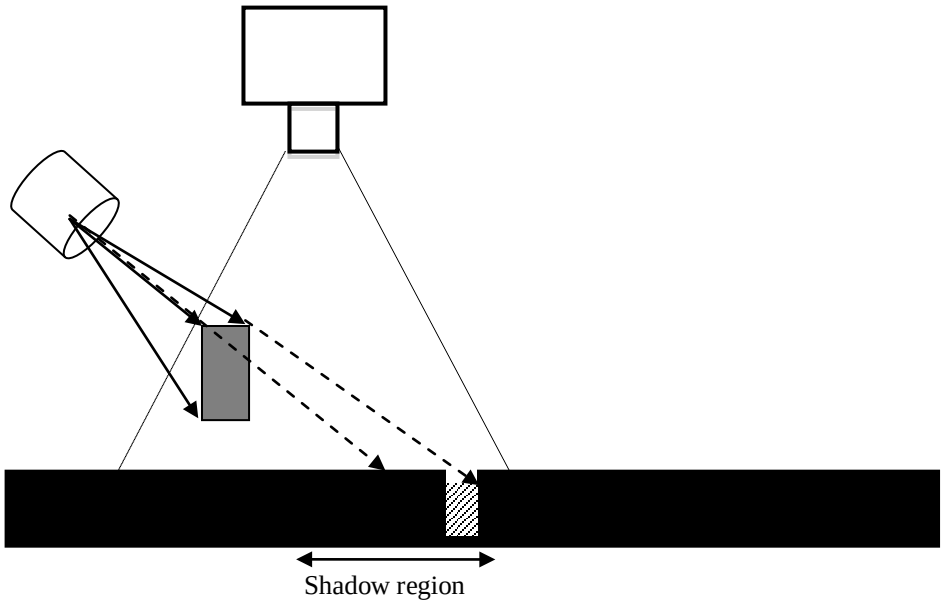

Figure 4.26: Base model of narrow crack in the surface

As can be seen from Figure 4.26, light cannot reach the bottom of the crack surface and therefore, the shadow border will not be formed as it did in the previous cases. As a result, the crack remains totally dark and therefore the crack edge is presumed by the camera as the shadow border. It is clear that in such case, the distance at which the presumed shadow edge is formed does not correspond to the depth of the crack. Though the depth calculated would differ from the actual depth of the crack, the information is not irrelevant in the scope of the application, as it does indicate the presence of a depression in the surface and thus identify the need to treat the surface.In this case study the crack was modeled as a narrow

rectangular depression in the surface with a depth of 1.5 cm. A sample image of the shadow profile over the crack is shown in Figure 4.27.

Figure 4.27: Sample image of shadow over the crack

The edge profile of the sampled image is shown in Figure 4.28.

Figure 4.28: Edge profile of sampled image

The images are sampled over a given interval, and the 3D profile is constructed following the generation of the point cloud. The images below showcase the point cloud and reconstructed model (Figures 4.29 and 4.30).

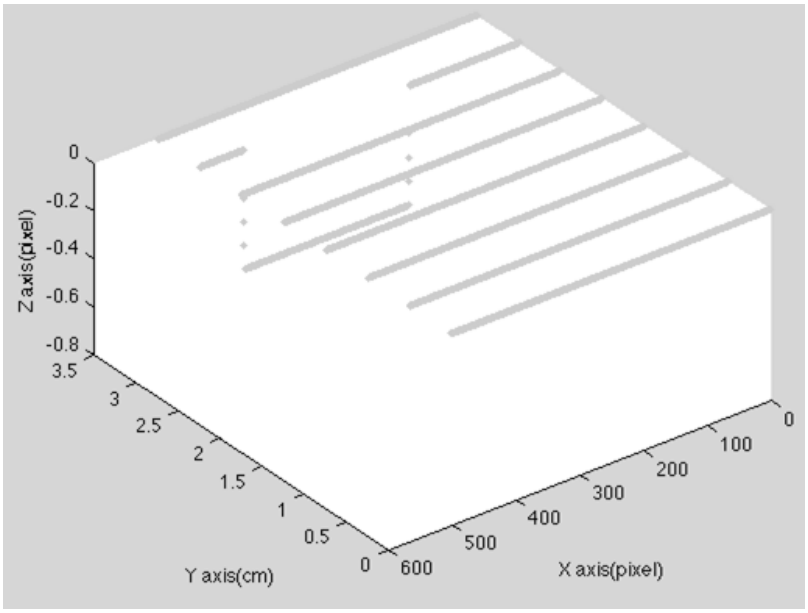

Figure 4.29: Point cloud of surface

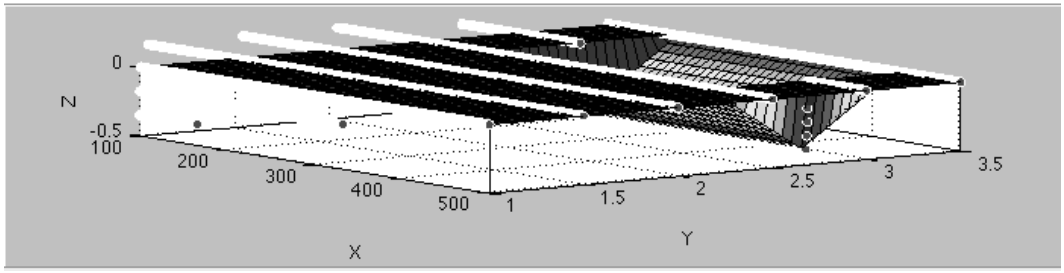

Figure 4.30: 3D reconstruction of the surface

The maximum depth of the crack calculated by shadow profilometry was found to be 0.5 cm. However the crack was modeled as a depression of 1.5 cm. The point cloud is compared against the original points of the corresponding section in the base model. By comparing the results of different sections of the surface with the original data, the maximum, minimum, average error and standard deviation was determined as shown in Table 4.4.

Table 4.4: Validation results of case 5

Maximum Error	:	1.1 cm
Minimum Error	:	1 cm
Average Error	:	0.72 cm
Standard Deviation	:	0.45

In practice, depressions such as those represented by the crack in this case, are treated by the application of mud. Owing to the difference between the calculated value and the actual depth of the crack, the amount of mud required would not be accurate. However, this is not very critical because, the applied mud would settle into the depths of the crack. As the mud has not covered the entire depth of the crack, a depression would still be present and would turn up in subsequent evaluation of the surface. Subsequent layers of mud can be applied until the region is found to be free from any depression.

4.2 Sensitivity Analysis

The case studies discussed in this chapter are based on the light source being incident at an angle of 45 degrees. The image processing algorithm uses the angle of incidence of the light source as an input for computing the deviation of a surface from flatness. This section describes how the variation of the angles of incidence would affect the accuracy of the model. Test cases were run on the model for the angles of 35^0, 40^0, 45^0, 50^0 and 55^0. The results were

compared and an analysis was drawn between the maximum error, average error and the standard deviation, which is illustrated in Figure 4.31.

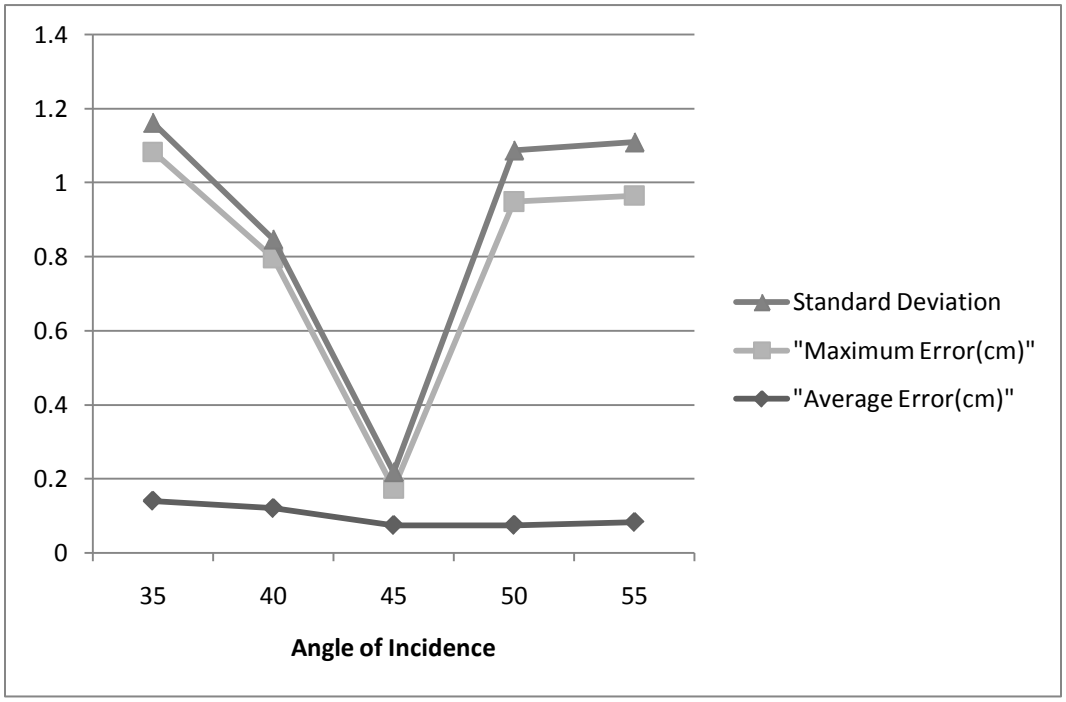

Figure 4.31: Sensitivity Analysis

At an angle of incidence of 45^0, the results were found to be more accurate than those calculated at the remaining angles. The shadow edge was found to closely follow the surface profile when the light source was directed at an angle of 45^0.

Chapter 5: Conclusions

5.1 General Conclusions

The growing interest in the industrialization of construction process promotes opportunities for automation. Automation brings improvement in quality and productivity of construction processes, while reducing workers exposure to hazardous work environments. The integration of robotics in interior finishing works, such as sanding and painting of drywalls is a relatively new concept. Progressing to a stage where fully autonomous robots are used for interior finishing works requires intermediate steps; namely surface profiling.

The understanding of the surface geometry is one such important step in the development of a fully autonomous system. Sensory technology has been around for decades, but its adoption to the construction process is relatively new. In an industry which is conservative in accepting changes, there is a need to provide solutions to automation which are easy to implement and of lower cost. One such method used for surface profiling, is shadow profilometry. The use of shadows for tracing a surface profile has been demonstrated in the wood and rock industry. This thesis has described a theoretical concept of shadow profilometery to profile the surface of an installed drywall. A shadow was cast over the area under consideration, and the shadow profile was captured as a 2D image by a camera. Digital image processing techniques of edge detection and interpolation were utilized for identifying regions that deviate from a flat surface. A 3D reconstruction of the surface provided information of parameters such as the

height and depth of these regions. The algorithm proposed in this research was tested across different case scenarios and the results were found to be encouraging. The main contribution of this research is the development of an algorithm for the purpose of identifying and quantifying surface deviations in a drywall. The algorithm utilizes existing methods and integrates them for the use of profiling the surface of a drywall for the purpose of sanding. Using a 3D modeling environment, the algorithm was tested across various case scenarios, each of which depicted a different surface profile. The cases considered were the following, a flat surface, a surface with an elevation, an electric socket-like depression cut into the surface, and a surface with a nail hole. The images of the shadow profile of different regions of the surface, were processed using the Sobel edge algorithm, and the traced edges where processed using the procedure described in the thesis. The 3D reconstruction of the surface from the point cloud was tested using the linear interpolation. The results obtained from simulations are found to be encouraging for the purpose of profiling a drywall surface which is to be sanded. Regions with curved surface profiles as demonstrated by case study 2 (Surface with elevation) and case study 4 (Surface with a nail hole), exhibit more deviations from the actual data. In these case studies, it was noted that the surfaces having an elevated profile obstructed the light from reaching regions of lower elevation, thereby creating an extra shadow apart from the one cast by the curtain. The computational accuracy could be further increased by defining a region of interest during image processing which comprises only that region showcasing the edge of the shadow profile.

5.2 Research Contributions

The contributions of this research are summarized as follows:

- The introduction of automated technology for drywall sanding.
- The introduction of shadow profilometry as a method of profiling the drywall surface.
- The successful simulation of shadow profilometry for surface profiling.
- The successful 3D reconstruction of the surface.

5.3 The Limitations of the Proposed Method

The limitations of this research are discussed as follows:

- The research treats the drywall as a single unit. The equations will vary when considering corner surfaces between two drywalls.
- In practice the accuracy of the system discussed, is greatly depended on the sharpness of the shadow. Interference from other light sources may result in blurriness of the shadow profile and will affect the accuracy of the proposed method.

5.4 Recommendations for Future Research

The proposed system promises scope for further research, primarily in the areas listed below.

- Experimental validation of the method.
- In the test setup, the shadow profile of the different sections of the surface is captured by the software. The distance between each section is

maintained as constant. In practice, the difference between each section is controlled by the mechanism which moves the sensor across the surface. The current system can be extended to incorporate a control by an overhead railing or a robotic arm, which is in turn synchronized with the overhead camera.

- Integration of the sensor into a robotic arm and design of an autonomous system for surface profiling.

.

References

Arai, T. (2005). “Robotics and Automation in Japanese Construction Industries.” International Symposium on Automation and Robotics in Construction (ISARC), Ferrara, Italy ,

Balaguer, C. and Abderrahim, M. (2008). “Trends in Robotics and Automation in Construction, Robotics and Automation in Construction.” IN-TECH, 1-20

Bernold, L.E. (1987). “Automation and robotics in construction: A challenge and change for an industry in transition.” International Journal of Project Management: The Journal of the International Project Management Association, 5(3), 155–160.

Bock, T. (2004). “Construction robotics and automation: past-present-future.” World Automation Congress, Proceedings June 28 2004-July 1, 2004.

Bock, T. (2007). “Construction robotics”, Autonomous Robot 22(3), 201–209.

(CII) Construction Industry Institute. (2003). “Breakthrough process and charter”, Breakthrough Strategy Committee (BTSC) Document 2003-2, The University of Texas at Austin, Austin, TX.

Elbehiery, H. , Hefnawy, A. , and Elewa, M. (2005). “Surface Defects Detection for Ceramic Tiles Using Image Processing and Morphological Techniques”, 3World Enformatika Society Conference on Computer, Electrical, and Systems Science, and Engineering, Istanbul, Turkey , 158–162.

Griffiths, B. J., Middleton, R. H. and Wilkie, B. A. (1994). “A Review of Light

Scattering for the Measurement of Surface Finish." International Journal of Production Research, Issue 11 November 1994 , pages 2683 - 2694

Haas, C., Skibviewski, M., and Budny, E. (1995). "Robotics in civil engineering." Microcomputers in Civil Engineering, Vol.10, No. 5, pp. 371–381.

Hagman, O. (1997). "Multivariate prediction of wood surface features using an imaging spectrograph." Holz Roh Werkst, 55:377– 382

Huynh, V. M. and Fan , Y. (1992). "Surface-texture measurement and characterization with applications to machine-tool monitoring." The International Journal of Advanced Manufacturing Technology Volume 7, Number 1, 2-10

Islam, A., Akhter, S., Mursalin, T. E. (2006). "Automated Textile Defect Recognition System using Computer Vision and Artificial Neural Networks." Proceedings World Academy of Science, Engineering and Technology, Volume 13, , ISSN:1307-688.

Islam, N., Parkin, R., Jackson, M.,Mueller, P. (2007). "A Novel Surface Profile Measurement System", AU J.T. 10(0):203-209

Kahane, B. and Rosenfeld, Y. (2004). "Balancing human and robot integration in building tasks." Computer-Aided Civil and Infrastructure Engineering, 19(6):393-410.

Maerz, N. H. Franklin, J. A. and Bennett, C. P. (1990). "Joint roughness measurement using shadow profilometry", International Journal of Rock Mechanics and Mining Science and Geomechanics, Abstract 27, pp. 329–343.

Maerz, N. H., and Hilgers, M. C. (2010). “A method for matching fractured surfaces using shadow profilometry.” Third International Conference on Tribology and Design 2010, Algarve, Portugal, pp. 237-248.

McDonald, K.A. (1978). “Lumber defect detection by ultrasonic’s.” Research Paper FPL 311. Forest Products Laboratory, Forest Service, USDA, Madison, Wis.

Miller, A. K., Esswein, E. J. and Allen, J. (1997). “Health hazard evaluation report 94-0078-2660”, NIOSH HETA 94-0078-2660 [cited 2010 Dec 16] Accessible online at http://www.cdc.gov/niosh/hhe/reports/pdfs/1994-0078-2660.pdf.

Neelamkavil, J. (2009). “Automation in the Prefab and Modular Construction Industry.” International Symposium on Automation and Robotics in Construction, Austin, Tex.

Poppy, W. (1994),”Driving forces and status of automation and robotics in construction in Europe.” Proceedings of 11th International Symposium of Automation and Robotics in Construction, Brighton, U.K., 215-222.

Roushdy, M. (2006). “Comparative study of edge detection algorithms applying on the grayscale noisy image using morphological filter.” Graphics, Vision and Image Processing Journal, vol. 6, pp17–23.

Sandak, J., and Tanaka, C. (2005). “Evaluation of surface smoothness using a light-sectioning shadow scanner.” Journal of Wood Science 51(3): 270-310

Seppä, J. and Heikkilä, R. (2009). “Automation of road maintenance -

Development of a roughness measurement system for the quality control of gravel roads." International Symposium on Automation and Robotics in Construction, Austin, Texas.

Sherrington, I. and Smith, E. H. (1988). "Modern measurement techniques in surface metrology: part II-optical instruments." Wear 125 289-308

Skibniewski, M., and Hendrickson, C. (1988). "Analysis of robotic surface finishing work on construction site." Journal of Construction Engineering and Management, ASCE, 1141, 53–68.

Skibniewski, M. J., and Russell, J. S. (1989). "Robotic applications to construction." AACE Cost Engineering Journal, 31(6),10-18.

Son, H., Kim, C. Kim, H., Heon, S. and Kim, M.K. (2009). "Trend Analysis of Research and Development on Automation and Robotics Technology in the Construction Industry", KSCE Journal of Civil Engineering, Volume 14, Number 2, 131-139, DOI: 10.1007/s12205-010-0131-7

Tam, V.W.Y., Tam, C. M., Zeng, S. X. and Ng, W.C.Y. (2007). "Towards adoption of prefabrication in construction", Building and Environment (10), pp. 3642–3654.

Vincent, O.R. and Folorunso, O. (2009). "A Descriptive Algorithm for Sobel Image Edge Detection". Informing Science & IT Education Conference (InSITE)

Whitehouse, D.J. (1987). "Surface Metrology Instrumentation", Journal of Physics, p. 1145.